NASA-CR-184,286

NASA-CR-184286
19920011193

CONTRACT NAS8-36471

Final Report: Part IV

CHEMICAL REACTION OF ATOMIC OXYGEN WITH EVAPORATED FILMS OF COPPER

Principal Investigators: A. T. Fromhold and J. R. Williams
Graduate Research Assistant: B. C. Gibson
Department of Physics
Auburn University, AL 36849

June 30, 1990

Prepared for

George C. Marshall Space Flight Center
Marshall Space Flight Center, Alabama 35812

CONTRACT NAS8-36471

Final Report: Part IV

CHEMICAL REACTION OF ATOMIC OXYGEN WITH EVAPORATED FILMS OF COPPER

Principal Investigators: A. T. Fromhold and J. R. Williams
Graduate Research Assistant: B. C. Gibson
Department of Physics
Auburn University, AL 36849

June 30, 1990

Prepared for

George C. Marshall Space Flight Center
Marshall Space Flight Center, Alabama 35812

CONTRACT NAS8-36471

Final Report: Part IV

CHEMICAL REACTION OF ATOMIC OXYGEN WITH EVAPORATED FILMS OF COPPER

Principal Investigators: A. T. Fromhold and J. R. Williams
Graduate Research Assistant: B. C. Gibson
Department of Physics
Auburn University, AL 36849

June 30, 1990

Prepared for

George C. Marshall Space Flight Center
Marshall Space Flight Center, Alabama 35812

ABSTRACT

Evaporated copper films have been exposed to an atomic oxygen flux of 1.4×10^{17} atoms/cm^2-sec at temperatures in the range 285 to 375°F (140 to 191°C) for time intervals between 2 and 50 minutes. Rutherford backscattering spectroscopy (RBS) was used to determine the thickness of the oxide layers formed and the ratio of the number of copper to oxygen atoms in the layers. Oxide film thicknesses ranged from 50 to 3000 Å (*viz.*, 0.005 to 0.3 μm, or equivalently, 5×10^{-9} to 3×10^{-7} m); it was determined that the primary oxide phase was Cu_2O. The growth law was found to be parabolic [$L(t) \propto t^{1/2}$], in which the oxide thickness L(t) increases as the square root of the exposure time t. The analysis of the data is consistent with either of the two ***parabolic growth laws*** derived by Fromhold. (The **thin-film parabolic growth law** is based on the assumption that the process is diffusion controlled, with the space charge within the growing oxide layer being negligible. The **thick-film parabolic growth law** is also based on a diffusion-controlled process, but it is assumed that space-charge neutrality prevails locally within very thick oxides.) In the absence of a voltage measurement across the growing oxide, a distinction between the two mechanisms cannot be made, nor can growth by the diffusion of neutral atomic oxygen be entirely ruled out. The activation energy for the reaction is of the order of 1.1 eV (*viz.*, 1.76×10^{-19} joule, or equivalently, 25.3 kcal/mole).

N92-20435#

TABLE OF CONTENTS

LIST OF FIGURES

LIST OF TABLES

I. INTRODUCTION

Ultraviolet radiation and low molecular densities in the earth's atmosphere at altitudes corresponding to low earth orbits are conducive to creating and sustaining atomic oxygen concentrations at these altitudes. Under conditions of normal solar activity, concentrations ranging from 10^6 atoms/cm^3 at an altitude of 600 kilometers to 10^{10} atoms/cm^3 at 200 kilometers have been measured[1]. Spacecraft at these altitudes have been shown to experience fluxes of atomic oxygen ranging in orders of magnitude from 10^{14} to 10^{16} atoms/cm^2–sec[2,3]. Atomic oxygen is much more reactive than the diatomic molecule ordinarily experienced at sea–level range altitudes and presents a severe corrosion problem for long duration space vehicles in low earth orbit. Extensive efforts have been made to better understand and reduce the detrimental effects of atomic oxygen on satellite components. The work presented herein represents a small part of this effort.

A facility existing on the Auburn University campus allows for the exposure of sample materials to a known atomic oxygen flux, providing a ground–based simulation of the phenomenon experienced in lower earth orbit. The atomic oxygen source, located in the Space Power Institute under the supervision of Dr. Charles Neely, is capable of producing atomic oxygen fluxes of the order 10^{17} atoms/cm^2–sec under controlled conditions of exposure time and sample temperature.

Thin films of evaporated copper having thicknesses between 2500Å and 3000Å were deposited on silicon wafer substrates by resistive heater evaporation. These samples were exposed to the atomic oxygen flux, and the resulting oxide layers were studied using available thin film techniques.

Several surface and thin film analytical techniques are available on campus for the analysis of these exposed materials, including a Rutherford backscattering spectroscopy (RBS) facility located in Leach Nuclear Science Center. The facility employs a 3 MeV Dynamitron linear accelerator to produce a highly collimated monoenergetic beam of $^4He^+$ particles which can be directed to a sample material. The particles scatter from the nuclei of the target material, and a small number of these particles is detected at a known scattering angle and are classified according to their recoil energies. The backscattered energies compose the abscissa of an RBS spectrum, and the number of particles detected at each measured energy (i.e. the scattering yield) is plotted along the ordinate.

The energy lost by the backscattered particle is indicative of the species of atom from which it scattered and the depth to which the particle penetrated prior to scattering into the solid angle of the detector. Analysis of the energy loss provides depth information for the sample. The yield at a particular energy (or depth in the sample) is related to the density of scattering centers at this depth so that information regarding the relative concentrations of various species as a function of depth can be assessed. The application of RBS supplies information at depths up to 5 microns beneath the sample surface.

Sample analysis allowed the determination of the chemical phase of the oxide layer formed on each sample and provided a set of oxide layer thicknesses corresponding to a constant atomic oxygen flux for varying temperatures and exposure times. These data were then compared to a theoretical expression describing the oxide formation as a function of exposure time and sample temperature. Least squares fits to the data resulted in the determination of an activation energy and rate constant of the copper/atomic oxygen interaction.

Scanning electron microscopy (SEM) was also used on a small number of thicker oxide layers for which the RBS spectra suggested the possibility of surface damage or deterioration. The changes in texture observed in the photographs can be directly correlated to changes observed in the RBS spectra.

II. THEORY

Rutherford Backscattering Concepts

Rutherford backscattering spectroscopy (RBS) is based on the elastic Coulomb scattering of an incident charged projectile particle of known energy by the nucleus of a target atom. The projectile particle recoils with an energy indicative of both the depth to which the projectile penetrated the sample before scattering and the species from which it scattered. The following is a discussion of the theory of Rutherford backscattering which can be used to obtain both qualitative and quantitative information about a sample under analysis.

A 3 MeV Dynamitron accelerator is used to generate a highly collimated, monoenergetic beam of $^4He^+$ particles which is introduced into a scattering chamber where the beam strikes the target sample under analysis. Details of the experimental arrangement may be found beginning on page 45 of Chapter III (EXPERIMENTAL PROCEDURE).

The incoming beam of particles strikes the sample at normal incidence, and a small fraction of these particles recoils into a solid angle Ω at an angle θ with respect to the direction of the incident beam. These scattered particles are detected with a silicon surface barrier detector. A schematic representation of this arrangement is presented in figure 1.

The detector detects each backscattered particle as an isolated event, and a multichannel analyzer records the number of particles detected at each energy interval over some reasonable range. The energy range is divided into a number of

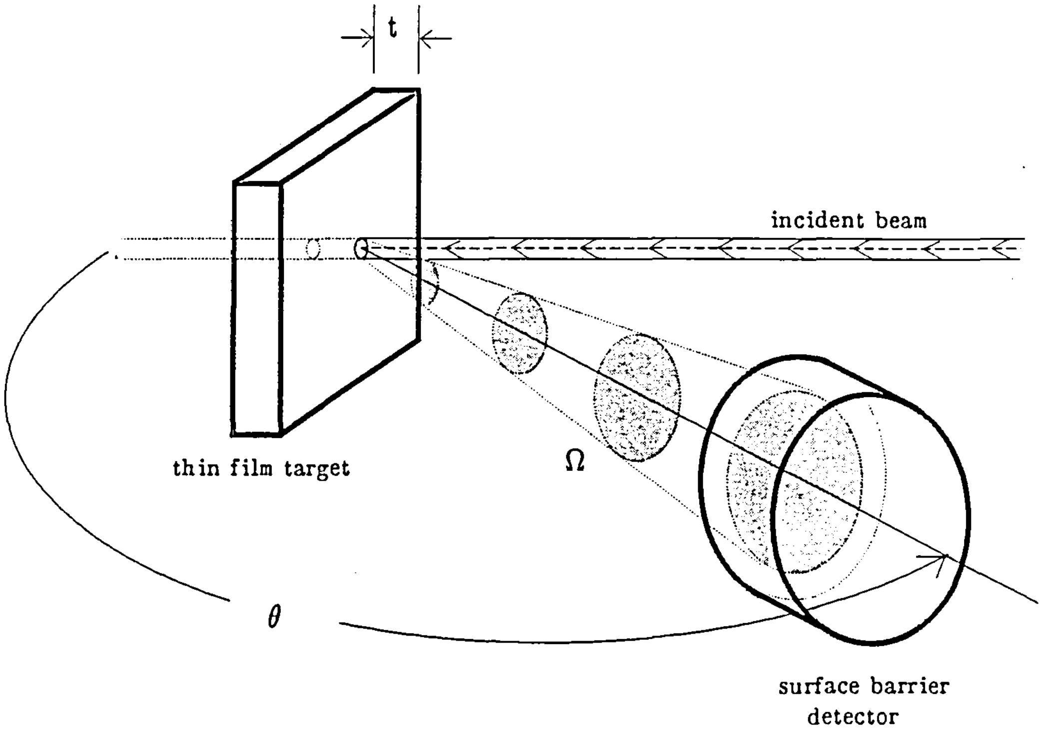

Figure 1. Particle beam incident on a thin solid film target of thickness t. A fraction of the recoiling particles scatters into the detector (solid angle Ω) at an angle θ with respect to the incident beam direction.

intervals equal to the number of channels available on the multichannel analyzer. Thus an RBS spectrum is comprised of the number of counts, or yield, versus the channel, or energy interval, within which each counted particle energy lies. A typical spectrum is shown in figure 2.

Scattering Cross Section

The ordinate or yield axis of an RBS spectrum such as that shown in figure 2 is governed by the differential Coulomb scattering cross section $\frac{d\sigma}{d\Omega}$. Nuclear contributions to scattering may be neglected for low energy incident particles which cannot overcome the Coulomb potential. For a total number of incident particles Q, the differential scattering cross section gives the number of detected particles dQ which scatter from a target of areal number density N_{area} into a differential solid angle $d\Omega$ subtended by the detector window. The volume number density N_{vol} of a uniform target of thickness t such as that shown in figure 1 is

$$N_{area} = t\, N_{vol} \tag{2.1}$$

Thus $\frac{d\sigma}{d\Omega}$ is given by[4]

$$\frac{d\sigma}{d\Omega} = (1/tN_{vol})\left[\frac{dQ/d\Omega}{Q}\right]. \tag{2.2}$$

The average differential scattering cross section $\left\langle\frac{d\sigma}{d\Omega}\right\rangle$ is then given by

$$\left\langle\frac{d\sigma}{d\Omega}\right\rangle = (1/\Omega)\int_{\Omega} \frac{d\sigma}{d\Omega}\, d\Omega. \tag{2.3}$$

For a very small detector solid angle Ω, $\frac{d\sigma}{d\Omega}$ is approximately constant over the

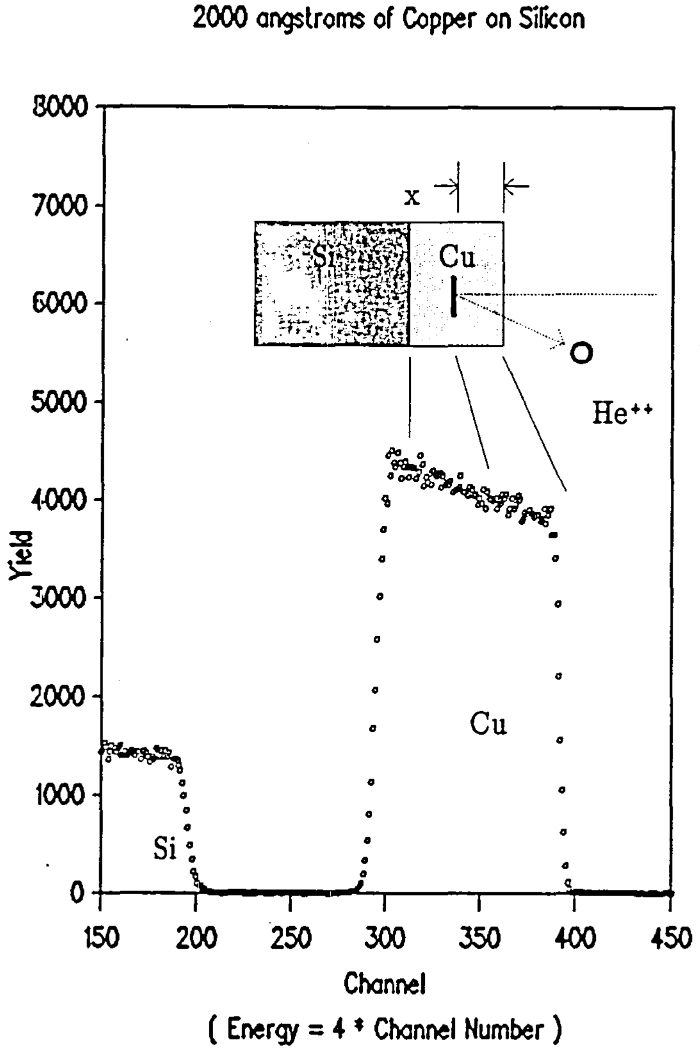

Figure 2. Rutherford backscattering spectrum of copper on silicon with sample diagram inlay. The spectrum shows the relation of spectrum peak width to sample depth.

detector face, and

$$\sigma \equiv \left\langle \frac{d\sigma}{d\Omega} \right\rangle \rightarrow \frac{d\sigma}{d\Omega}. \qquad (2.4)$$

Here the standard notation as found in most RBS literature for the average differential scattering cross section σ is defined and will be the notation used henceforth. The yield of an RBS spectrum is the total number of scattered particles ΔQ detected at an angle θ by a detector with a solid angle Ω and is given

$$\Delta Q = \sigma \, \Omega \, Q \, N_{vol} \, t. \qquad (2.5)$$

The calculation of the differential cross section for the scattering of a projectile particle can be accomplished by treating the path of the particle as an orbit about the target nucleus in a center–of–mass (cm) system[4]. The force acting on the two nuclei can be very well described by the Coulomb repulsion if the closest approach of the projectile is small compared to the Bohr radius but large compared to the radius of the nuclei involved. For an incident particle of mass M_1 and atomic number Z_1 and a target atom of mass M_2 and atomic number Z_2, the differential cross section is[5]

$$\frac{d\sigma}{d\Omega} = \left[\frac{Z_1 Z_2 e^2}{4\sin(\theta_{cm}/2)}\right]^2 \qquad (2.6)$$

where e is the electronic charge, and θ_{com} is the scattering angle with respect to the center–of–mass coordinate system. For the case in which $M_1 << M_2$, this transforms into the laboratory reference frame as[4]

$$\frac{d\sigma}{d\Omega} = \left[\frac{Z_1 Z_2 e^2}{4E}\right]^2 \frac{4}{\sin^4\theta} \frac{\{[1-((M_1/M_2)\sin\theta)^2]^{\frac{1}{2}} + \cos\theta\}^2}{[1-((M_1/M_2)\sin\theta)^2]^{\frac{1}{2}}}. \qquad (2.7)$$

Kinematic Factor

The abscissa or energy axis of an RBS spectrum is primarily governed by the kinematic factor K_{M_2}. The kinematic factor is defined as the ratio of the recoil energy E_{recoil} of the projectile to the incident energy $E_{incident}$ and carries the subscript of the target mass M_2 such that

$$E_{recoil} \equiv K_{M_2} E_{incident}. \tag{2.8}$$

Consider the hard sphere model of a single projectile particle of mass M_1, energy E_0 and velocity v_0 colliding elastically with a stationary target atom of mass M_2. Let the particle recoil at an angle θ with velocity v_1 and energy E_1 while the target atom is ejected in the direction ϕ with velocity v_2 and energy E_2 as shown in figure 3. For the general case, the energy E_i and momentum p_i of a particle having mass M and velocity v_i are given by

$$E_i = \tfrac{1}{2} M v_i^2$$

and (2.9)

$$p_i = M v_i.$$

The conservation equations for energy and linear momentum can be written using equations (2.9) as

$$\tfrac{1}{2} M_1 v_0^2 = \tfrac{1}{2} M_1 v_1^2 + \tfrac{1}{2} M_2 v_2^2, \tag{2.10}$$

$$M_1 v_0 = M_1 v_1 \cos\theta + M_2 v_2 \cos\phi, \tag{2.11}$$

and

$$0 = M_1 v_0 \sin\theta - M_2 v_2 \sin\phi. \tag{2.12}$$

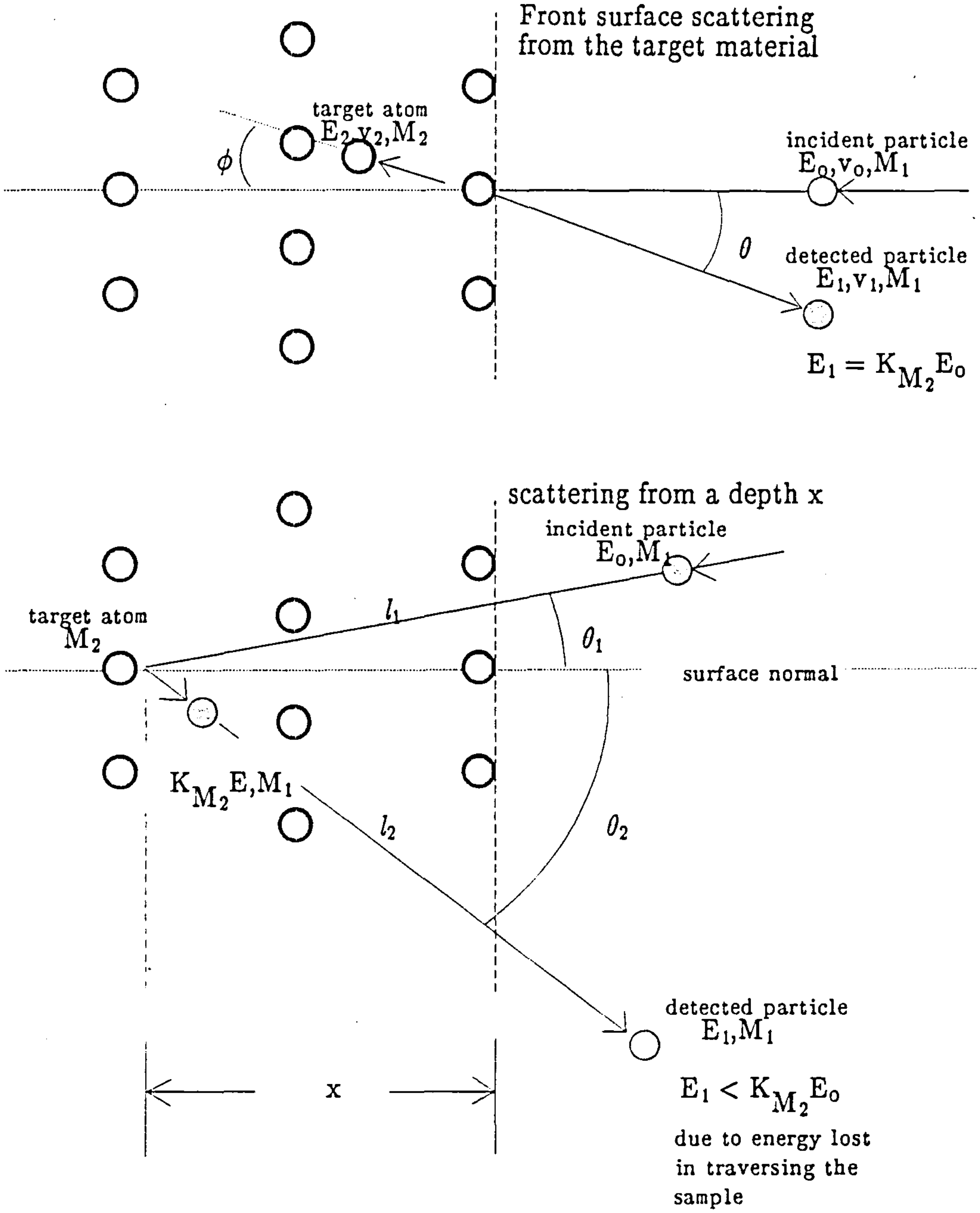

Figure 3. Hard sphere model of front surface scattering and scattering from a depth x beyond the front surface of the target material.

The ratio $\frac{v_1}{v_0}$ can be obtained from the system of equations (2.10) through (2.12) in terms of M_1, M_2 and θ

$$\frac{v_1}{v_0} = \left[\frac{(M_2^2 - M_1^2 \sin^2\theta)^{\frac{1}{2}} - M_1\cos\theta}{M_1 + M_2}\right]. \tag{2.13}$$

Combining equations (2.8) and (2.9), the kinematic factor can be shown to be the square of expression (2.13)

$$K = \left[\frac{v_1}{v_0}\right]^2 = \left[\frac{[1 - (M_1/M_2)^2\sin^2\theta]^{\frac{1}{2}} + (M_1/M_2)\cos\theta}{1 - (M_1/M_2)}\right]^2 \tag{2.14}$$

where equation (2.13) has been rewritten in terms of M_1/M_2. The detected energy of a particle recoiling from a front surface target atom having mass M_2 will be

$$E_1 = K_{M_2}E_0. \tag{2.15}$$

Energy Loss in a Target Sample

The energy of the detected particle scattered from the same species target atom at some depth in the sample will be less than the energy resulting from front surface scattering. This is due to the reduction of the particle velocity (and thus the particle energy) as it penetrates the sample before scattering at a depth x as shown in figure 3. The instantaneous energy loss is actually a function of the energy itself, in that the lower the incident energy, the greater the energy loss will be after travelling some particular distance.

Specific energy loss. The specific energy loss dE/dx as a function of the instantaneous energy E is written

$$\frac{dE}{dx}(E) = \lim_{\Delta x \to 0} \frac{\Delta E}{\Delta x} \tag{2.16}$$

where ΔE is the change in energy over some distance Δx traversed in the target medium. The energy E at an arbitrary depth x can then be expressed as

$$E(x) = E_0 - \int_0^x \left[\frac{dE}{dx}(E)\right] dx. \tag{2.17}$$

with $E_0 = E(x=0)$.

Stopping cross section ε. The specific energy loss is a collective effect specific to a material having a certain composition and atomic number density. A related concept is the stopping cross section. It is a measure of the stopping potential of the individual atoms composing the sample. For a beam of incident particles of cross sectional area A penetrating to a depth Δx in a target sample having atomic number density N_{vol}, the total number of particles N_0 in the volume defined by A and Δx is

$$N_0 = (A\ \Delta x)\ N_{vol} \tag{2.18}$$

such that the areal density N_{area} is

$$N_{area} = \frac{(A\Delta x)N_{vol}}{A} = \Delta x\ N_{vol}. \tag{2.19}$$

The areal density increases linearly with Δx, and from

$$\Delta E = \left[\frac{dE}{dx}\right] \Delta x, \tag{2.20}$$

it is evident that ΔE also increases linearly with Δx. Thus N_{volume} is proportional to dE/dx such that

$$\left[\frac{dE}{dx}(E)\right] \equiv \varepsilon(E)\, N_{volume} \tag{2.21}$$

where the proportionality constant ε at energy E is defined as the stopping cross section. The stopping cross section is most commonly expressed in units of eV–cm^2/atom. Fifth order polynomial curve fits for a $^4He^{++}$ projectile in the energy range 0.4 to 4 MeV have been compiled for target elements with atomic numbers of 4 through 92 by Zeigler et al[6]. This compilation was used in the data analysis performed for this research. Refer to page 49 of Chapter III for further details.

<u>Scattering at a Depth x</u>

Because dE/dx is a function of the energy E at a depth x and E(x) is the quantity of interest in equation (2.17), the integral cannot be evaluated as presented. This difficulty is sidestepped by regarding x as a function of E, rather than E a function of x, so that

$$dx = \frac{dx}{dE}(E) \cdot dE. \tag{2.22}$$

The depth x as a function of energy E now takes the integral form

$$x = \int_{E}^{E_0} \frac{dx}{dE} \cdot dE = \int_{E}^{E_0} \left[\frac{dE}{dx}\right]^{-1} dE. \tag{2.23}$$

The integral still cannot be evaluated unless the functional form of dE/dx is known. Several possibilities exist for handling this problem. For fast particles, a common method is to approximate the integrand of equation (2.23) by a constant value of dE/dx evaluated at some representative energy E_{approx} which is between the front surface energy E_0 and the energy E before scattering at depth x. For the general case of a particle travelling a path length l into a medium, the integral becomes

$$E_0 - E_l = l \left[\frac{dE}{dx}\right]\Bigg|_{E_{approx}} \tag{2.24}$$

where E_0 is the energy at the start of path l in the medium, and E_l is the energy of the particle after travelling a distance l into the medium. For the geometry depicted in figure 3, let

$$l_1 = \frac{x}{\cos\theta_1} \text{ and } l_2 = \frac{x}{\cos\theta_2}$$

such that

$$E_0 - E = \frac{x}{\cos\theta_1}\left[\frac{dE}{dx}\right]\Bigg|_{E^{in}_{approx}} \tag{2.25}$$

and

$$K_{M_2}E - E_1 = \frac{x}{\cos\theta_2}\left[\frac{dE}{dx}\right]\Bigg|_{E^{out}_{approx}} . \tag{2.26}$$

for the inward and outward paths of the projectile particle, respectively. The superscripts ^{in} and ^{out} refer to the representative energies along the inward and outward paths of figure 3. The values for E and $K_{M_2}E$ are not known but can be eliminated by solving the system of equations (2.25) and (2.26) for the difference ΔE in detected energies[4].

$$\Delta E \equiv K_{M_2}E_0 - E_1 = \left[\frac{K_{M_2}}{\cos\theta_1} \left[\frac{dE}{dx}\right]\Bigg|_{E^{in}_{approx}} + \frac{1}{\cos\theta_2} \left[\frac{dE}{dx}\right]\Bigg|_{E^{out}_{approx}} \right] x \tag{2.27}$$

where $K_{M_2}E_0$ is the energy detected from a front surface scattering, and E_1 is the energy detected after scattering from an atom at a depth x in a sample. Equation (2.27) can be rewritten in terms of the stopping cross section ε using equation (2.21)

$$\Delta E \equiv K_{M_2}E_0 - E_1 = \left[\frac{K_{M_2}}{\cos\theta_1} \varepsilon(E^{in}_{approx}) + \frac{1}{\cos\theta_2} \varepsilon(E^{out}_{approx}) \right] N_{vol}\, x. \tag{2.28}$$

The equation can be further reduced by defining the bracketed term as the stopping cross section factor $[\varepsilon]$ such that

$$[\varepsilon] = \left[\frac{K_{M_2}}{\cos\theta_1} \varepsilon(E^{in}_{approx}) + \frac{1}{\cos\theta_2} \varepsilon(E^{out}_{approx}) \right]. \tag{2.29}$$

Then

$$\Delta E = [\varepsilon]\, N_{vol}\, x. \tag{2.30}$$

The correlation between the width of an energy peak and a layer thickness for a sample such as that shown in figure 2 can be determined using equation (2.30).

Energy Approximations for Spectrum Analysis

The accuracy of the approximation discussed in the previous section is dependent upon the accuracy of the approximated energies E^{in}_{approx} and E^{out}_{approx}. Two common approximations are the *surface energy approximation* and the *mean* *energy approximation.* A modification of the mean energy approximation is the *symmetrical mean energy approximation.*

Surface energy approximation. Perhaps the simplest approximation for the E_{approx} is the assumption that this energy remains constant at E_0 along the inward path of the particles and remains constant at $K_{M_2}E_0$ along the outward path. That is,

$$E^{in}_{approx} = E_0 \quad \text{and} \quad E^{out}_{approx} = K_{M_2}E_0. \tag{2.31}$$

This approximation is known as the surface energy approximation and is valid for fast incident particles and thin sample layers. This approximation becomes less reliable as the depth increases because the particle energy falls farther and farther below the front surface energy as the particle progresses through the sample. For a 2 MeV ^{4}He particle, the approximation is reliable for depths up to about 3000Å.

Mean energy approximation. For more accurate thickness calculations at greater depths, the energies for stopping cross section factor calculations can be assumed to be the average values

$$E^{in}_{approx} = \tfrac{1}{2}(E_0 + E) \quad \text{and} \quad E^{out}_{approx} = \tfrac{1}{2}(E_1 + K_{M_2}E). \tag{2.32}$$

The value for E, the energy just prior to scattering, is not known and must be determined in some manner. Several techniques may be used to estimate values for E. These include iteration methods, Taylor series approximations, or the use of various functional forms for dE/dx[4].

Symmetrical mean energy approximation. The simplest method of calculating E in the mean energy approximation is to make the assumption that the energy difference ΔE as defined in equation (2.28) is divided equally between the inward and outward paths. Upon further assumption that the kinematic factor K_{M_2} is close to unity (a good approximation for heavy target nuclei), the values for E^{in}_{approx} and E^{out}_{approx} reduce to[4]

$$E^{in}_{approx} = E_0 - \tfrac{1}{4}\Delta E$$

and (2.33)

$$E^{out}_{approx} = E_1 + \tfrac{1}{4}\Delta E.$$

Composite Samples

The assumption made throughout the previous sections is that the target sample is composed of a single species of atom. Rutherford backscattering would be severely limited if application of the technique were limited to elemental samples. However using Bragg's rule, the equations developed thus far can be extended to composite samples. Relative concentrations of the various elements composing the sample at a given depth can be assessed in this manner, allowing the application of RBS techniques to composite materials such as alloys, compounds and diffusant materials.

Bragg's rule. Bragg's rule states that a compound sample A_mB_n consisting of m atoms of element A and n atoms of element B will have a composite stopping cross section which is the weighted sum of the stopping cross sections of the individual elements in the compound

$$\varepsilon^{A_mB_n} = m\varepsilon^{A} + n\varepsilon^{B} \tag{2.34}$$

where $\varepsilon^{A_mB_n}$ is the stopping cross section of the composite, and ε^{A} and ε^{B} are the cross sections of the respective elements A and B.

Stopping cross section factor for composites samples. Direct substitution of equation (2.34) into (2.29) yields

$$\left[\varepsilon\right]_{A}^{A_mB_n} = m\left[\varepsilon\right]_{A}^{A} + n\left[\varepsilon\right]_{A}^{B}. \tag{2.35}$$

for the stopping cross section factor. The superscript represents the sample medium which the projectile particle traverses and so defines the stopping cross sections $\varepsilon(E_{approx}^{in})$ and $\varepsilon(E_{approx}^{out})$ to be used in equation (2.29). The detected particle for a composite sample A_mB_n will have been scattered from either element A or B as noted by the subscript in equation (2.35). The target atom also affects the approximated energy E_{approx}^{out} used in calculating $\varepsilon(E_{approx}^{out})$. Thus the stopping cross section factor for a particle travelling through a medium A_mB_n and scattering from element B would retain the same *superscript* as in equation (2.35) but have *subscript* B.

Thickness measurements in a composite sample. The depth relation (2.30) for elemental samples can be extended to the composite A_mB_n by applying equations (2.34) and (2.35). Equation (2.30) becomes

$$\Delta E = K_A E_0 - E_1 = \left[\varepsilon(E)\right]_{A}^{A_mB_n} N_{vol}^{AB}\, x \tag{2.36}$$

where N^{AB}_{vol} is the composite number density, and the subscript for the kinematic factor K_A corresponds to that of the stopping cross section factor $\left[\varepsilon\right]^{A_mB_n}_{A}$.

Relative concentration of species. Rutherford backscattering is not sensitive to the chemical composition of composite samples in that it cannot directly discern between chemical compounds and mixtures having the same elemental ratios. However, insight into chemical phase can be gained by determining the relative concentration of species $\frac{n}{m}$ for a compound sample A_mB_n.

A single channel height H^A_A of a single channel in an RBS spectrum corresponding to a sample composed of a single element A (see figure 2) results from particles detected from within some thickness region δt. With a normally incident beam (θ_1=0), equation (2.5) applies and gives the relation

$$H^A_A = \sigma(E)\,\Omega\,Q\,N^A_{vol}\,\delta t. \tag{2.37}$$

The superscript of H^A_A refers to the sample composition, and the subscript denotes the species from which the particles scatter. The density N^A_{vol} refers to the atomic number density of the species A from which the particles are being scattered. The region δt can be expressed using equation (2.30) as

$$N^A_{vol}\,\delta t = \frac{\delta E}{\left[\varepsilon\right]^A_A}. \tag{2.38}$$

This expression can be combined with equation (2.37) to yield

$$H^A_A = \sigma(E)\,\Omega\,Q\,\frac{\delta E}{\left[\varepsilon\right]^A_A}. \tag{2.39}$$

A similar expression to that of equation 2.38 for a compound sample A_mB_n such as the Cu_2O sample shown in figure 4 can be written as

$$N_{vol}^{A_mB_n}\,\delta t = \frac{\delta E}{\left[\varepsilon(E)\right]_A^{A_mB_n}}. \tag{2.40}$$

A sample with molecular density $N_{vol}^{A_mB_n}$ is composed of m atoms of A and n atoms of B such that

$$N_{vol}^{A} = m\, N_{vol}^{A_mB_n}. \tag{2.41}$$

Combining this with equation (2.40) yields an expression for the peak height

$$H_A^{A_mB_n} = \sigma(E_0)\,\Omega\,Q\,\frac{m\,\delta E}{\left[\varepsilon(E)\right]_A^{A_mB_n}}. \tag{2.42}$$

Substituting equation (2.35) into equation (2.42) and dividing equation (2.39) by the resultant expression produces the following expression for the ratio of peak heights from two spectra – one from a sample containing a single element A and the other from a compound sample containing the same element A[1].

$$\frac{H_A^A}{H_A^{A_mB_n}} = 1 + \frac{n}{m}\,\frac{\left[\varepsilon(E)\right]_A^B}{\left[\varepsilon(E)\right]_A^A} \tag{2.43}$$

The ratio of species $\frac{n}{m}$ can then be written as

$$\frac{n}{m} = \left[\frac{H_A^A}{H_A^{A_mB_n}} - 1\right]\frac{\left[\varepsilon(E)\right]_A^A}{\left[\varepsilon(E)\right]_A^B}. \tag{2.44}$$

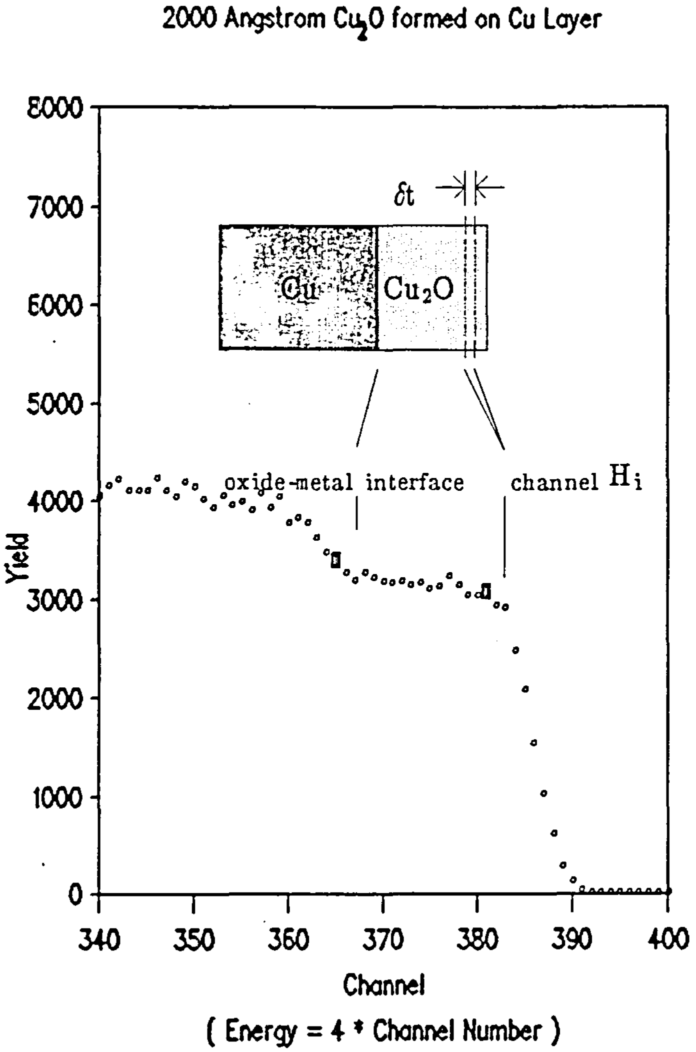

Figure 4. Rutherford backscattering spectrum of copper oxide on copper with corresponding sample inlay. The diagram inlay shows the relation of a single channel yield to the corresponding position in the sample.

Again, this does not conclusively determine the chemical formula of a compound but the ratio indicates the most probable phase. For instance, if comparison of a copper oxide film and a copper film yields a value of $\frac{n}{m} = 0.5$, a chemical formula of Cu_2O could be assumed. A value $\frac{n}{m} = 1.0$ would indicate a CuO phase.

Oxide Layer Growth

The depth of a metal oxide layer formed at the surface of a pure metal due to exposure to a constant flux of atomic oxygen varies as a function of the duration of the exposure and the temperature of the metal during the exposure time. An equation will be developed for the thickness of an oxide layer as a function of exposure time and temperature.

Uncharged Particle Diffusion Theory and Time Dependence of Oxide Growth

The laws governing the diffusion process are Fick's law and the continuity equation for diffusing atoms. Fick's first law states that the flux J of a an uncharged diffusant material is directly proportional to the gradient of the concentration $\nabla C(x)$ of the diffusant in the parent material and is written[7]

$$J = -D(T)\nabla C(x) \tag{2.45}$$

where D is a proportionality constant known as the diffusion coefficient – being constant for constant temperature T and is usually expressed in units of cm^2/s. The minus sign is a convention for positive values of D(T) to show the flux moves in the direction of decreasing concentration. The concentration C(x) has units of diffusant atoms/cm^3.

The continuity equation is a generality of Fick's second law and states that the partial derivative of the concentration with respect to time $\frac{\partial C}{\partial t}$ and the divergence of the flux $\nabla \cdot \mathbf{J}$ sum to zero[7]

$$\frac{\partial C}{\partial t} + \nabla \cdot \mathbf{J} = 0. \tag{2.46}$$

In a steady state solution for the concentration, $\partial C/\partial t$ is zero. For the one dimensional case in which the concentration varies only in the x direction but is uniform about the x–axis as shown in figure 5, the steady state solution becomes

$$\frac{\partial J}{\partial x} = 0 \tag{2.47}$$

which implies that the flux J is a constant. Substitution into equation 2.45 yields

$$J = -D(T)\frac{\partial C(x)}{\partial x}. \tag{2.48}$$

Integration of equation (2.48) over the oxide layer depth L of figure 5 gives

$$\int_0^L J dx = -\int_0^L D(T)\frac{\partial C(x)}{\partial x} dx. \tag{2.49}$$

The left hand side integrates to yield LJ while the right hand integral becomes

$$-\int_0^L D(T)\frac{\partial C}{\partial x}(x) dx = -\int_{C(0)}^{C(L)} D(T) dC = D(T)\Big[C(0) - C(L)\Big]. \tag{2.50}$$

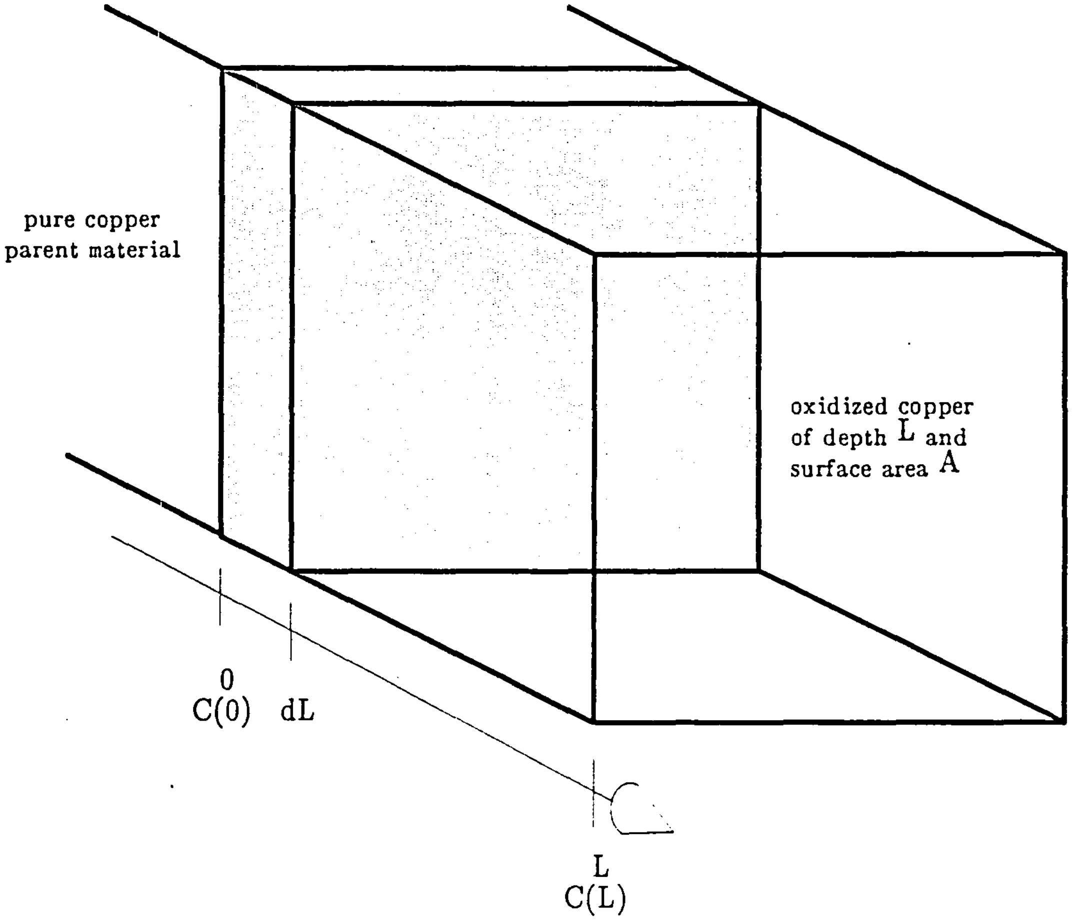

Figure 5. Macroscopic model of laterally uniform oxide of thickness L forming on a pure copper parent material.

Equating left and right hand sides and solving for J gives

$$J = D(T)\frac{C(0) - C(L)}{L}. \tag{2.51}$$

Consider the flux of atoms traversing the length L of the oxide layer. Assume that as each atom reaches the interface it reacts to form an oxide of the same phase as that of the traversed layer, and that this oxide phase contains one oxygen atom per molecule. The volume of the oxide layer is then increased by the effective volume R of one molecule of oxide for every atom that reaches the interface. This effective volume is the average real space occupied by a molecule of oxide. Thus for n atoms of oxygen reaching the interface, the volume of the oxide layer is increased by nR. For an oxide layer growing uniformly about the x axis with area A as shown in figure 5, the layer volume is equal to the area A multiplied by the depth of the oxide L such that AL = nR. Differentiating this with respect to time gives

$$\frac{d}{dt}(AL) = A\frac{dL}{dt} = \frac{d}{dt}(nR) = R\frac{dn}{dt}. \tag{2.52}$$

Solving for dL/dt and recognizing that the flux is the number of particles traversing a unit area per unit time yields the relation

$$\frac{dL}{dt} = R\,\frac{1}{A}\,\frac{dn}{dt} = RJ(L) \tag{2.53}$$

where R is the inverse of the atomic density of the oxide.

The value of R has a constant magnitude but the sign may differ according to the coordinate system chosen. The value of dL/dt will be positive because the oxide increases during the diffusion process, regardless of the mechanism controlling the flux. However, the flux will be positive or negative depending on the chosen coordinate system. Thus the value of R will have the same sign as that of the flux to keep dL/dt positive. Specifically, for a metal atom or ion diffusing from the metal–metal oxide interface, with the coordinate system of figure 5, both the flux and the R value will be positive. Likewise, for oxygen diffusing from the oxide–oxygen boundary, R will be negative.

Combining equations 2.51 and 2.53 yields the differential equation

$$\frac{dL}{dt} = RJ(L) = \frac{R\ D}{L}\left[C(0) - C(L)\right]. \tag{2.54}$$

The differential equation can be solved by the method of separation of variables and integration to yield

$$\int_0^L L dL = \int_0^t RD\left[C(0) - C(L)\right] dt \tag{2.55}$$

which integrates to give

$$L^2(t) - L^2(0) = 2RD\left[C(0) - C(L)\right]t.$$

Where RD[C(L) – C(0)] in this expression is defined as the rate constant.

Evaluating this expression and solving for L under the assumption that the thickness L(t=0) = 0 gives the following expression for the time dependence of the growth of the oxide layer

$$L(t) = \left[\ 2RD\left[C(0) - C(L)\right]\ \right]^{\frac{1}{2}} t^{\frac{1}{2}}. \tag{2.56}$$

Note that the concentration C(0) is the concentration of diffusant atoms at the metal/oxide interface. From the left hand side of equation (2.56), L is seen to be a function of time, although C(0) is assumed to remain constant at the interface under steady state conditions.

Temperature dependence of the diffusion coefficient D. The diffusion coefficient D is usually assumed to have an Arrhenius temperature dependence

$$D(T) = D_0 e^{-U/kT} \tag{2.57}$$

where D_0 is a temperature independent constant characteristic of a particular diffusant/parent system, k is Boltzmann's constant and U is the activation energy. In general, the activation energy is a measure of the average energy of the potential barrier a diffusant atom must overcome in changing from one state to another. Energy must be supplied, often in the form of heat, in order for the diffusing species to overcome this barrier[8]. For the case of the growth of an oxide layer, this barrier may be the energy required to move an oxygen atom from one site in the sample to another, or it may be the energy required to move a copper ion from one site to another, eventually reaching a surface site. The source(s) of this barrier is difficult to determine experimentally.

Substitution of equation 2.57 into equation 2.56 produces the expression[9]

$$L(T,t) = \left[2\, R\, D_0 \left[C(L) - C(0) \right] \right]^{\frac{1}{2}} t^{\frac{1}{2}}\, e^{-U/2kT}. \tag{2.58}$$

This equation demonstrates the parabolic growth law for uncharged particle diffusion — showing temperature and exposure time dependences.

Charged Particle Diffusion

The presence of electric fields inside the growing oxide layer may contribute to the growth of the oxide layer in the case of ionic diffusant species. The one dimensional diffusion equation for the s^{th} charged diffusant species then becomes[10]

$$J_s = -D_s(T)\frac{\partial C_s(x)}{\partial x} + \mu_s E(x) C_s(x). \qquad (2.59)$$

where μ_s is the ion mobility of the s^{th} charged species and E(x) is the electric field at a location x in the system. Even though no external electric field is applied, there is a natural tendency for the charge currents of the oppositely charged species to set up a field. This is formalized in Fromhold's coupled currents condition – an approach which argues that the quasi–stationary state of an oxide growth is the situation for which the electric field has a value producing a net charge transport[10] of zero, or

$$\sum_{s=0}^{r} Z_s \, e \, J_s = 0. \qquad (2.60)$$

This implies that the sum of all charged particle currents, both ionic and electronic, sum to zero in the medium. The contributions from surface charge in thin films and from localized space charge for thicker films constitute sources of the electric field in the oxide medium. This leads to an equation for the growth rate of an oxide on a metal. The mechanisms and resulting oxide thickness equations will be developed in the remainder of this chapter for the cases of both thin and thick films.

Charged particle diffusion in thin films. For a charged diffusant species in an oxide medium so thin that space charge is negligible, the one dimensional expression for linear diffusion becomes[11]

$$J_s = -D_s(T)\frac{\partial C_s(x)}{\partial x} + \mu_s E_0 C_s \tag{2.61}$$

where μ_s is the ion mobility of the s^th^ species, and E_0 is the electric field within the oxide. Even in the absence of an external electric field, the coupled current condition leads to excess surface charges at the metal–oxide interface and the oxide–oxygen interface, and the charge distributions establish an internal electric field of sufficient strength to modify ionic/electronic currents through the oxide layer. The electric field is assumed to be homogeneous, independent of the position x in the oxide. The ion mobility μ_s and D_s are related by the Einstein relation[11]

$$Z_s e\, D_s = \mu_s k\, T \tag{2.62}$$

where $Z_s e$ is the s^{th} species charge.

Under the steady state assumption that J_s is not a function of the position x, and with assumptions of a homogeneous field E_0 and fixed boundary concentrations $C_s(0)$ and $C_s(L)$ for the diffusant species at the interfaces, equation 2.61 becomes a first order ordinary differential equation. Solving for dC_s/dx and multiplying by the integration factor $\exp(-\mu_s E_0 x/D_s)$, this equation becomes

$$\frac{d}{dx}[C_s \exp(-\mu_s E_0 x/D_s)] = -\frac{J_s}{D_s}\exp(-\mu_s E_0 x/D_s). \tag{2.63}$$

Integrating and solving for $C_s(x)$ gives

$$C_s(x) = \frac{J_s}{\mu_s E_o} + C_{so}\exp(\mu_s E_o x/D_s) \tag{2.64}$$

where C_{so} is a constant of integration having units of concentration. Evaluation of equation 2.64 at $x=L$ and $x=0$ yields a system of equations for which J_s and C_{so} are the unknowns.

$$C_s(L) = \frac{J_s}{\mu_s E_o} + C_{so}\exp(\mu_s E_o L/D_s) \tag{2.65}$$

and

$$C_s(0) = \frac{J_s}{\mu_s E_o} + C_{so}. \tag{2.66}$$

The simultaneous solution of equations 2.65 and 2.66 gives[11]

$$J_s = \mu_s E_o \left[\frac{C_s(L) - C_s(0)\exp(\mu_s E_o L/D_s)}{1 - \exp(\mu_s E_o L/D_s)}\right]$$

and

$$C_{so} = C_s(0) - \mu_s E_o \left[\frac{C_s(L) - C_s(0)\exp(\mu_s E_o L/D_s)}{1 - \exp(\mu_s E_o L/D_s)}\right]. \tag{2.67}$$

Substitution of equations 2.67 into equation 2.64 gives

$$\begin{gathered} C_s(x) = [C_s(L) - C_s(0)\exp(Z_s e E_o L/kT)/[1 - \exp(Z_s e E_o L/kT)] + \\ C_s(0) - C_s(L)\exp(Z_s e E_o x/kT)/[1 - \exp(Z_s e E_o L/kT)] \end{gathered} \tag{2.68}$$

Substitution of equation 2.67 into equation 2.60 and division by eE_0 gives[11]

$$\sum_{s=1}^{r}\{Z_s\mu_s[C_s(L) - C_s(0)\eta^{Z_s}]/[1 - \eta^{Z_s}]\} = 0 \tag{2.69}$$

where

$$\eta = \exp(eE_0L/kT). \tag{2.70}$$

Multiplying equation 2.69 by the product $\prod_{j=1}^{r}(1 - \eta^{Z_j})$ gives an algebraic expression for which the physically–meaningful roots η_0 must be real and positive since from equation 2.70[11]

$$E_0 = (kT/eL)\ln(\eta_0). \tag{2.71}$$

Because the coefficients of equation 2.69 are independent of L, the electric field E_0 can be seen from equation 2.71 to be inversely proportion to L(t). Substitution of equations 2.71 into 2.67 gives[11]

$$J_s = \mu_s \frac{kT\ln(\eta_0)}{eL(t)}\left[\frac{C_s(L) - C_s(0)\exp(Z_seE_0L/kT)}{1 - \exp(Z_seE_0L/kT)}\right]. \tag{2.72}$$

From the same arguments leading to equation 2.54 and with R_s being the volume of one molecule produced by a single ion of the s^th^ diffusant species,

$$\frac{dL}{dt} = R_s\, J_s(L) = \frac{\sum_{s=1}^{r}\chi_sR_s}{L(t)} \tag{2.73}$$

where

$$\chi_s = \mu_s \frac{kT\ln(\eta_0)}{e}\left[\frac{C_s(L) - C_s(0)\exp(Z_seE_0L/kT)}{1 - \exp(Z_seE_0L/kT)}\right] \tag{2.74}$$

is the coefficient of $1/L(t)$ in equation 2.72. Equation 2.72 leads (in similar fashion of equations 2.55 through 2.56) to

$$L(t) = [2 \sum_{s=1}^{l} R_s \chi_s]^{\frac{1}{2}} t^{\frac{1}{2}}, \tag{2.75}$$

Fromhold's thin film parabolic law demonstrating the parabolic time dependence for the growth of an oxide layer. In this equation, the rate constant is defined as $\sum_{s=1}^{l} R_s \chi_s$, where l is the number of diffusing ionic species.

Charged particle diffusion in thick films. As oxide growth progresses, the oxide thickness may become large enough that space charge considerations must be accounted for. It has been shown through mathematical modeling that the interior region of a thick oxide film has the property of local space charge neutrality[12]. Stated mathematically this condition is[13]

$$\sum_{s=1}^{r} Z_s e\, C_s = 0. \tag{2.76}$$

Also, the electric field in the oxide is no longer homogeneous, such that the ordinary linear diffusion equation must retain the form of equation 2.59,

$$J_s = -D_s(T)\frac{\partial C_s(x)}{\partial x} + \mu_s E(x) C_s(x). \tag{2.77}$$

The coupled currents condition (equation 2.60) is still applicable and can be combined with equation 2.77 to give an expression for the electric field as a function of x[13]

$$E(x)=\frac{\sum_{s=1}^{r} Z_s e\ D_s\ dC_s/dx}{\sum_{s=1}^{r} Z_s e\ \mu_s\ C_s}. \tag{2.78}$$

For two diffusing species composed of (1) an ion and (2) its electronic counterpart, equations 2.78, 2.76 and the derivative form of equation 2.76

$$\sum_{s=1}^{r} Z_s e\, dC_s/dx = 0 \tag{2.79}$$

can be combined to give

$$E(x) = \left[\frac{D_1 - D_2}{\mu_1 - \mu_2}\right] \frac{1}{C_s(x)} \frac{dC_s(x)}{dx} \tag{2.80}$$

for s = 1,2. Direct substitution of equation (2.80) into (2.77) gives the result[12]

$$J_s = -\frac{\mu_1 D_2 - \mu_2 D_1}{\mu_1 - \mu_2} \frac{dC_s(x)}{dx}. \tag{2.81}$$

Let the interior region of the oxide over which this equation is valid be defined as the region beginning at $x=\delta^*$ from the metal–oxide interface and extending to $x=L^*$, as shown in figure 6. Multiplying equation 2.81 by dx, integrating from $x'=\delta^*$ to x=x and solving for J_s gives[13]

$$J_s = \frac{\mu_1 D_2 - \mu_2 D_1}{\mu_1 - \mu_2} \frac{C_s(\delta^*) - C_s(x)}{x - \delta^*}. \tag{2.82}$$

Evaluation at $x=L^*$ gives an expression for the particle current J_s in terms of the boundaries of the interior zone for which the assumptions leading to expression

2.82 are valid

$$J_s = \frac{\mu_1 D_2 - \mu_2 D_1}{\mu_1 - \mu_2} \frac{C_s(\delta^*) - C_s(L^*)}{L^* - \delta^*}. \tag{2.83}$$

The thickness L can be written in terms of the three zones as

$$\begin{aligned} L &= \delta^* + (L^* - \delta^*) + (L - L^*) \\ &\cong \Delta_1 + (L^* - \delta^*) + \Delta_3 \end{aligned} \tag{2.84}$$

where Δ_1 and Δ_3 are time independent quantities defined as[13]

$$\begin{aligned} \Delta_1 &= \lim_{L \to \infty} \delta^* \\ \Delta_3 &= \lim_{L \to \infty} (L - L^*). \end{aligned} \tag{2.85}$$

In the limit where the approximation of equation 2.84 holds[13],

$$(L^* - \delta^*) >> \Delta_1 + \Delta_3$$

such that

$$L(t) \cong L^* - \delta^*. \tag{2.86}$$

The problem now lies in relating the concentrations at the boundaries of the interior zone to the concentrations at the metal–oxide interface (x=0) and the oxide–oxygen interface (x=L). The assumption is made that the diffusant concentrations in the outer regions from x=0 to x=δ^* and from x=L^* to x=L (see

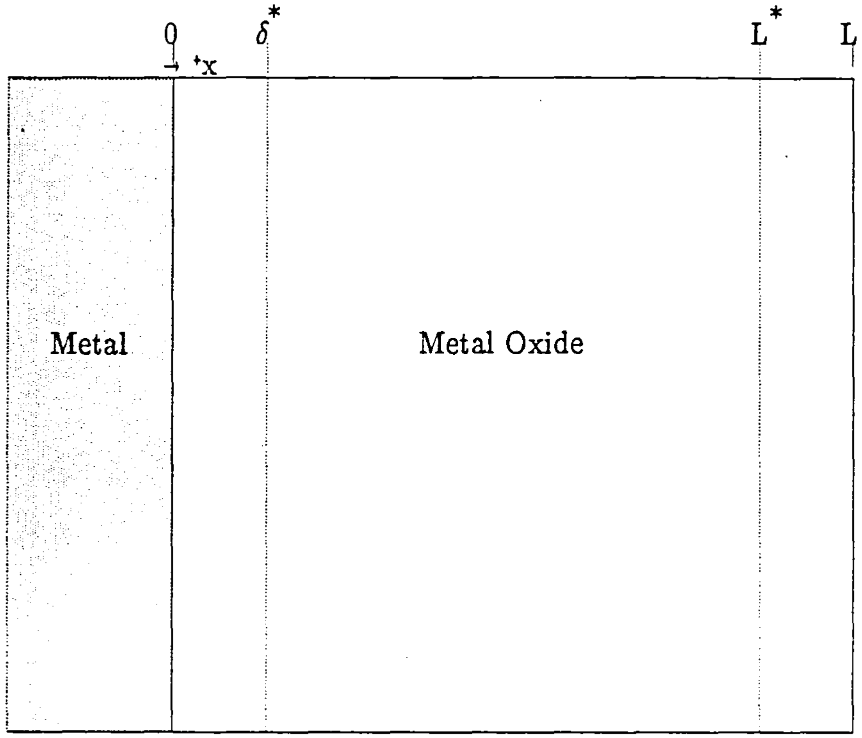

Figure 6. Diagram showing the boundaries δ^* and L^* of an oxide layer forming on a metal surface. These boundaries define the interior region of local space charge neutrality for thick oxide films.

figure 6) are concentrations in thermal equilibrium, in which case the Boltzmann distribution applies to relate the concentration at two points x and x′ by[13]

$$C_s(x) = C_s(x')e^{-\frac{U_s(x) - U_s(x')}{kT}} \qquad (2.87)$$

where $U_s(x)$ is the electrostatic energy $Z_seV(x)$ and V(x) is the potential difference. Letting x′=0, V(0)=0 and $x=\delta^*$, equation 2.87 becomes

$$C_s(\delta^*) = C_s(0)e^{-\frac{U_s(\delta^*)}{kT}} = C_s(0)e^{-\frac{Z_seV(\delta^*)}{kT}} . \qquad (2.88)$$

Applying the local space charge neutrality condition (equation 2.76) for a single ionic diffusant species (1) and its electronic counterpart (2) gives

$$Z_1eC_1(0)e^{-\frac{Z_1eV(\delta^*)}{kT}} + Z_2eC_2(0)e^{-\frac{Z_2eV(\delta^*)}{kT}} = 0 \qquad (2.89)$$

which can be solved for the potential $V(\delta^*)$ resulting in the expression[12]

$$V(\delta^*) = kT/e\,[Z_1 - Z_2]\ln\left[\frac{-Z_1C_1(0)}{Z_2C_2(0)}\right]. \qquad (2.90)$$

Substitution of this expression into equation 2.88 produces the expression of the concentration at $x=\delta^*$ [12]

$$C_s(\delta^*) = C_s(0)\left[\frac{-Z_1C_1(0)}{Z_2C_2(0)}\right]^{-Z_s/(Z_1-Z_2)} . \qquad (2.91)$$

The same methods used to develop equations 2.84 through 2.87 can be applied to obtain an approximate expression for the concentration $C(L^*)$ in terms of the concentration $C(L)$[12]

$$C_s(L^*) = C_s(L)\left[\frac{-Z_1C_1(L)}{Z_2C_2(L)}\right]^{-Z_s/(Z_1-Z_2)}. \qquad (2.92)$$

Now too, as in the preceding uncharged particle and thin film derivations, equation 2.53 still holds

$$\frac{dL}{dt} = RJ(L).$$

For the thick oxide films in which equation 2.86 is a good approximation and Δ_1 and Δ_3 are time independent

$$\frac{dL}{dt} = \frac{d(L^*-\delta^*)}{dt} \cong R_1J_1(L^*-\delta^*), \qquad (2.93)$$

and upon substitution of equation 2.82 into the above expression,

$$\frac{d(L^*-\delta^*)}{dt} = R_1\left[\frac{\mu_1D_2-\mu_2D_1}{\mu_1-\mu_2}\right]\frac{[C_1(\delta^*)-C_1(L^*)]}{(L^*-\delta^*)}. \qquad (2.94)$$

Because $L(t) \cong (L^* - \delta^*)$, equation 2.83 becomes

$$\frac{dL}{dt} = R_1\left[\frac{\mu_1D_2-\mu_2D_1}{\mu_1-\mu_2}\right]\frac{[C_1(\delta^*)-C_1(L^*)]}{L(t)}. \qquad (2.95)$$

Time integration of this expression from $t'=t_0$ to $t'=t$ gives yet another equation for oxide layer thickness which demonstrates a parabolic dependence on exposure time in Fromhold's thick oxide film law[13]

$$L^2(t) - L^2(t_o) = 2R_1\left[\frac{\mu_1 D_2 - \mu_2 D_1}{\mu_1 - \mu_2}\right][C_1(\delta^*) - C_1(L^*)](t - t_o) \tag{2.96}$$

where the rate constant is

$$R_1\left[\frac{\mu_1 D_2 - \mu_2 D_1}{\mu_1 - \mu_2}\right][C_1(\delta^*) - C_1(L^*)],$$

and the concentrations $C_1(\delta^*)$ and $C_1(L^*)$ are given in terms of the interface concentrations according to the respective equations 2.91 and 2.92. The thickness $L(t_o)$ must be large enough to support an interior region of space charge neutrality.

III. EXPERIMENTAL PROCEDURE

Analysis was performed on thin Cu film samples deposited on Si substrates. Rutherford backscattering spectra were taken of the freshly deposited Cu for the comparison studies with the oxide spectra and to detect impurities and physical defects. The Cu/Si systems were then exposed to a monatomic oxygen source with controlled temperature and atomic oxygen fluence. A second set of RBS spectra were then generated. Analysis of the spectra corresponding to the exposed and unexposed sample (or an unexposed sample representative of the particular set of prepared films) determined the oxide phase and layer thickness for each sample. Samples were analyzed in this manner to determine an equation governing the temperature– and time–dependence of the oxide layer growth for a particular oxygen flux. The following is a discussion of the sample preparation, data acquisition and data analysis including a description of the facilities used in each phase of the research.

Sample Preparation

Thin Copper Film Deposition

Thin copper films were deposited by resistive heating evaporation in a diffusion pumped vacuum system at a pressure less than 10^{-6} Torr. The deposition rate of 99.99975% pure copper wire was monitored by a deposition thickness monitor and was controlled by adjusting the resistive boat current to maintain a deposition rate of 10 ± 2 nm per second. The samples were stored under vacuum until the atomic oxygen exposures were performed.

Atomic Oxygen Exposure

Principles of operation of the atomic oxygen source. Atomic oxygen (O^3P) was generated in a glass atomic oxygen source located in the Space Power Institute at Auburn University. Nitric oxide (NO) enters the atomic oxygen source through a diffuser where it is titrated with monatomic nitrogen (N) gas. Diatomic nitrogen (N_2) is dissociated as it passes through a microwave discharge tube to produce the monatomic nitrogen gas as shown in figure 7. The nitric oxide and nitrogen combine according to the reaction

$$N + NO \rightarrow N_2 + O. \qquad (3.1)$$

The N_2 and O flow across the sample mounted on the sample probe in the direction of the pumping system. The ultimate pressure of the system is approximately 2×10^{-3} Torr with no gas flow. An enlarged view of the sample probe is presented in figure 8. The N_2 component produced is chemically inert and does not interact with the sample.

The titration process and consequently the pressure and atomic oxygen flux are governed by the flow meter settings for the nitric oxide and nitrogen gases introduced into the source. For normal use, the flow rate of the nitric oxide is set to correspond to a desired atomic oxygen flux and the nitrogen flow rate is then adjusted to bring the titration to endpoint. The overtitration of nitrogen gas into the source causes a second reaction in addition to (3.1).

$$N + N \rightarrow N_2 \qquad (3.2)$$

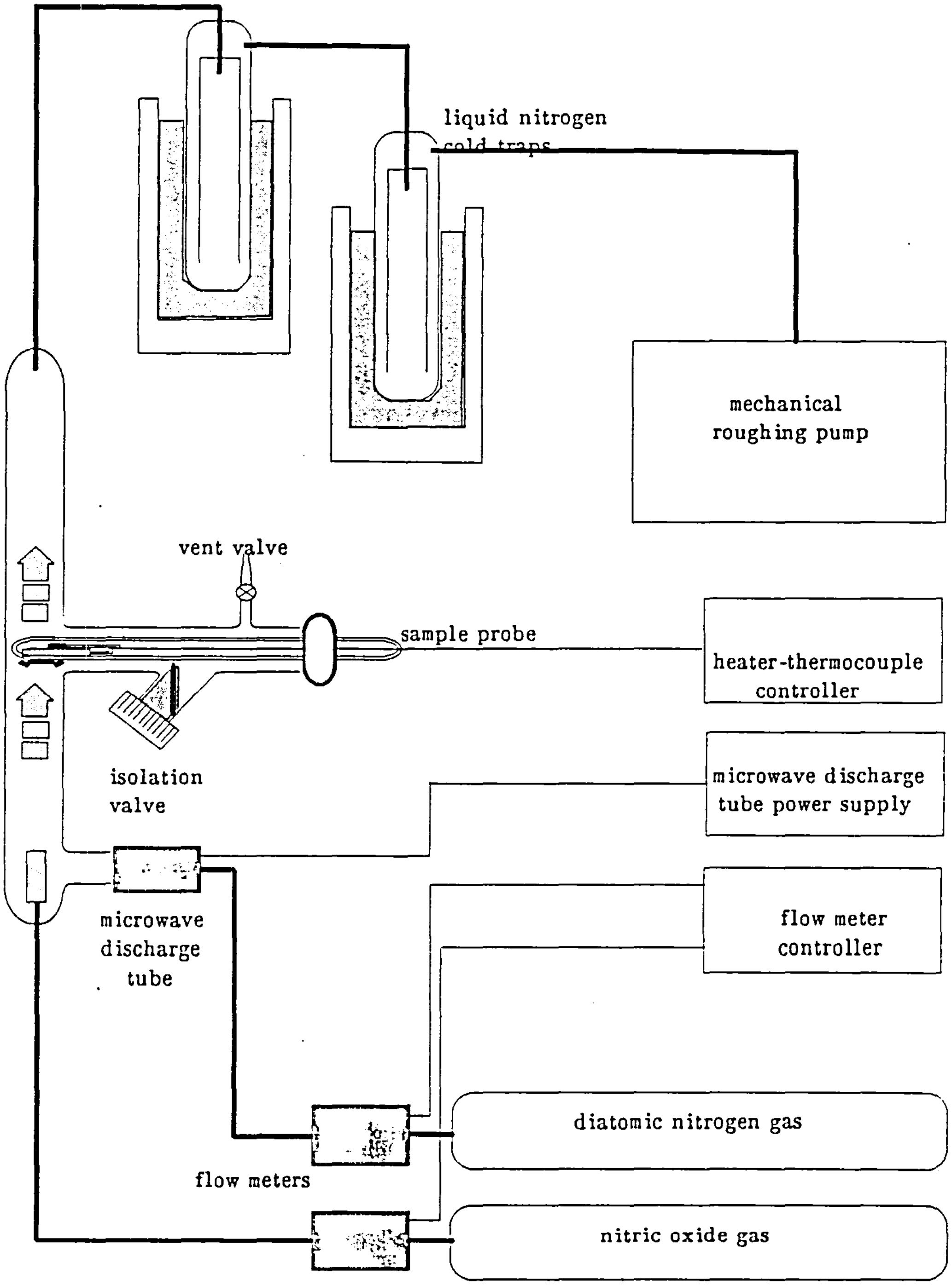

Figure 7. Diagram of the atomic oxygen source used to expose thin copper film samples to a preset flux of atomic oxygen with controlled exposure times and temperatures.

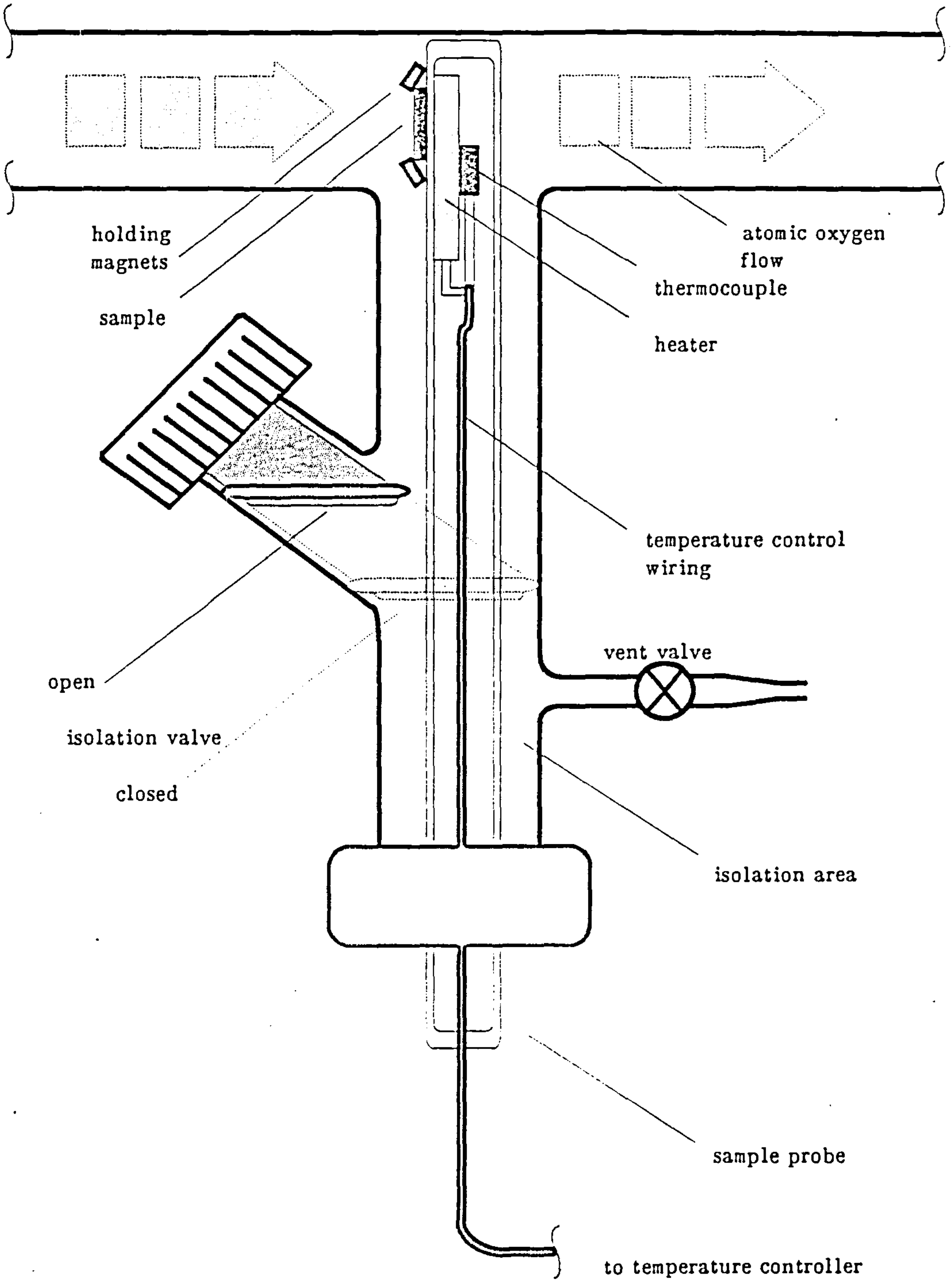

Figure 8. Magnified view of the sample probe of figure 7 as it is positioned in the atomic oxygen source.

This recombination reaction is chemiluminescent, emitting a photon with wavelength in the visible range ($\lambda \cong 5500$Å). Insufficient nitrogen gas leads to the reaction

$$\mathrm{N} + \mathrm{O} \rightarrow \mathrm{NO} \qquad (3.3)$$

which also emits a photon in the visible range ($\lambda \cong 4500$Å). Endpoint is achieved by adjusting the nitrogen flow rate until no visible light emission is observed which indicates that neither of the secondary reactions (3.2) and (3.3) are occurring.

The atomic oxygen flux can be calculated once the titration reaches endpoint. For example, a nitric oxide flow rate of 1.5 ml/min has a corresponding number of NO molecules per minute of

$$1.50\,\frac{\mathrm{ml\ NO}}{\mathrm{min}}\left[\frac{1\ \mathrm{mole}}{22414\mathrm{ml}}\right]\left[\frac{6.024\mathrm{x}10^{23}\mathrm{molecules}}{1\ \mathrm{mole}}\right] = 4.03\mathrm{x}10^{19}\,\frac{\mathrm{molecules}}{\mathrm{min}}$$

At titration endpoint, the only chemical reaction taking place is reaction (3.1), which states that one molecule of nitric oxide produces one atom of oxygen, thus the number of oxygen atoms flowing past the sample of figure 8 will be equal to the number of molecules of NO flowing into the source. For this example, there are then $4.03\mathrm{x}10^{19}$ O atoms/min flowing past the sample. The flow is restricted to a tube with a diameter of 2.5 cm. The corresponding flux for this example is then

$$4.03\mathrm{x}10^{19}\,\frac{\mathrm{O\ atoms}}{\mathrm{min}}\left[\frac{1\ \mathrm{min}}{60\ \mathrm{sec}}\right]\left[\frac{\pi\ (2.5\mathrm{cm})^2}{4}\right]^{-1} = 1.4\mathrm{x}10^{17}\,\frac{\mathrm{O\ atoms/cm^2}}{\mathrm{sec}}.$$

A heater/k–type thermocouple system placed in the tip of the sample probe (see figure 8) allows for temperature control of the sample under exposure.

Temperatures near the maximum for the system (200°C) can be held within ±3°C. Samples were held in place using two small disc magnets. The temperature controller had a solid state reference junction, alleviating the need for an ice bath temperature reference, although one was used during calibration.

Two cold traps were placed in series near the pump to avoid contamination of the system from backstreaming oil (see figure 7). Also, when in operation the system had a continual dry N_2 gas purge at a pressure of approximately 1.7 Torr. The gases used for the production of atomic oxygen were ultra pure research grade in order to prevent contamination due to water vapor.

Sample exposure using the atomic oxygen source. A flux of atomic oxygen was first established in the atomic oxygen source using 1.50 ml/min nitric oxide and titrating to endpoint with nitrogen gas The heater/thermocouple system was turned on and set to the desired temperature. The system was given approximately one hour to stabilize and fine adjustments were made on the flow meter controls to ensure an atomic oxygen flux of 1.4×10^{17} O atoms/cm^2/sec corresponding to the 1.50 ml/min nitric oxide flow. The samples were then fixed to the sample probe using the disc magnets and placed in the isolation area shown in figure 8 with the isolation valve closed. The isolation area was evacuated and the samples were allowed 10 minutes to reach thermal equilibrium. The samples were then introduced into the atomic oxygen flow for the desired exposure time. Upon completion of the exposure of a set of samples, the set was placed under vacuum to await Rutherford backscattering analysis. The nitric oxide flow meter was flushed and backfilled with dry argon gas to prevent unnecessary corrosion of the flow meter. Sample exposure times ranged from 2 to 50 minutes at probe temperatures of 149, 162, 177, 192 and 205°C.

Data Acquisition

Principles of Operation of the Rutherford Backscattering Facility

Rutherford backscattering spectroscopy is achieved in the laboratory by employing a 3 MeV Dynamitron linear accelerator. Electron emissions from a filament in the source of the accelerator ionize ^{4}He gas which is introduced into the source. These ions are extracted and accelerated through a 2 megavolt potential difference. After exiting the accelerator, an analyzing magnet directs the singly ionized $^4He^+$ at energy 2 MeV down the drift tube of the vacuum system and steers other ionized components away from this direction, thus producing a monoenergetic beam of $^4He^+$. The base operating pressure is about 1×10^{-8} Torr.

The beam of particles first encounters two vertical slits as it progresses down the drift tube as shown in figure 9. Beam current collected by these two slits is monitored and the accelerator potential adjusts slightly so as to minimize the beam current collected on the left and right slits by adjusting the curvature of the beam induced by the analyzing magnet, thus serving to center the beam horizontally in the drift tube.

The beam next passes through two sets of square apertures, one located immediately after the slit system and one located immediately before the scattering chamber as shown in figure 9. The two apertures serve to collimate the beam and reduce the beam area to a 0.02" square.

The beam strikes the sample at normal incidence and a fraction of the particles are detected at a scattering angle $\theta = 164^\circ$ (see figure 1). The detector is located 2.25 inches from the sample and subtends a solid angle of 9.8 ± 0.1 millisteradians. The signal from the detector passes through a preamplifier

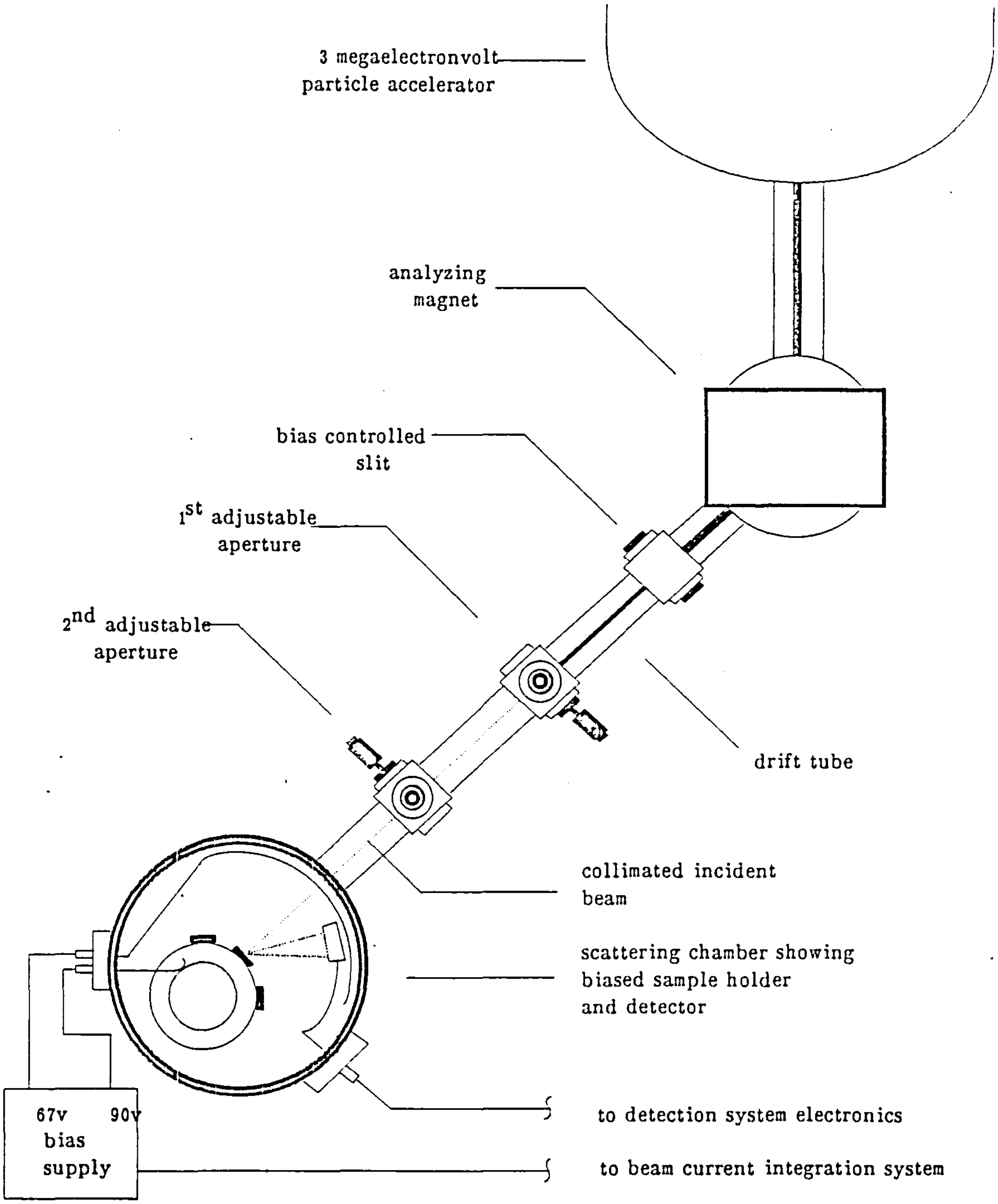

Figure 9. Schematic diagram of the Rutherford backscattering facility.

located at the scattering chamber. The amplifier output is then shaped by a main amplifier as shown in figure 10 and the resulting voltage pulses are processed by a personal computer equipped with a multichannel analyzer (MCA) card. Computer software allows for the display and disk storage of the generated RBS spectra[14].

A biasing system consisting of a faraday cup assembly described by Musket and Taajas was used in the chamber[15]. An isolated bias supply was used to bias the faraday cup at 67 volts and the sample holder at 90 volts. This procedure was followed in order to collect the charged particles entering the chamber and thus determine the number of He^+ particles incident on the sample. The beam current integration was accurate to within about 4%.

Generating Rutherford Backscattering Spectra

A collimated, 2 MeV beam of $^4He^+$ was used to irradiate samples in the scattering chamber. Energy calibration was established over the range of 0–2000 keV for the multichannel analyzer system using an ^{241}Am source and a precision pulse generator. The bias supply was connected to the Faraday cup, the sample holder, and to the input of the beam current integration system.

Each of twelve samples loaded in the chamber was successively placed in the beam at normal incidence for a beam current integration of 20,000 counts (one count corresponds to 6.25×10^8 He^+ particles) with an incident current of approximately 3 nA. The generated spectra were stored on disk for later analysis.

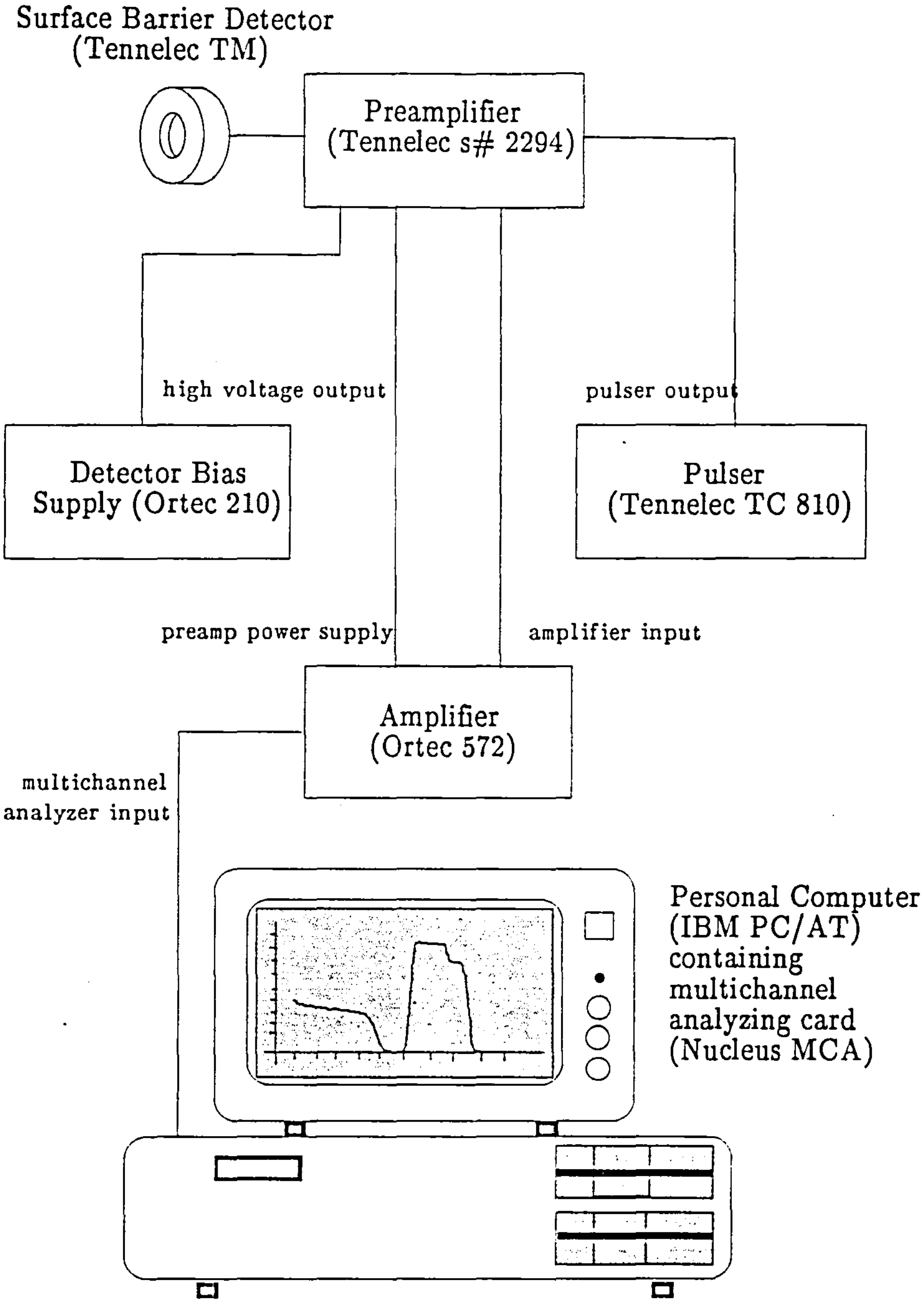

Figure 10. Diagram showing the detector electronics configuration. Specific electronics models utilized are parenthesized.

Data Analysis

Oxide Phase and Thickness Determination

The oxide phase was determined by comparing the height H^{Cu}_{Cu} of a single channel in the spectrum of an unexposed Cu film to the height $H^{Cu_mO_n}_{Cu}$ of the corresponding channel for the same sample after atomic oxygen exposure using equation (2.44)

$$\frac{n}{m} = \left[\frac{H^{Cu}_{Cu}}{H^{Cu_mO_n}} - 1 \right] \frac{\left[\varepsilon(E)\right]^{Cu}_{Cu}}{\left[\varepsilon(E)\right]^{O}_{Cu}} \tag{3.4}$$

where the stopping cross section factors $\left[\varepsilon(E)\right]^{Cu}_{Cu}$ and $\left[\varepsilon(E)\right]^{Cu}_{Cu}$ are defined by equation (2.29) using the notation of chapter II.

The value for $\frac{n}{m}$ was used to assign a chemical formula for the oxide compound formed on the sample under evaluation. The atomic density of the oxide $N^{Cu_mO_n}_{vol}$ was then taken from a compilation of tabulated values of oxide densities[16]. The depth L of the oxide was determined by substituting equation (2.35) into equation (2.36) using the numbers m and n and the atomic density as determined from the ratio to give

$$L = \frac{K_{Cu}E_0 - E}{N^{Cu_mO_n}_{vol} \left\{ m\left[\varepsilon(E)\right]^{Cu}_{Cu} + n\left[\varepsilon(E)\right]^{O}_{Cu} \right\}} . \tag{3.5}$$

The values for E used in equations 3.4 and 3.5 were approximated using both the front surface energy and the symmetrical mean energy approximations as outlined in Chapter I.

Computer software was written to incorporate equations 3.4 and 3.5 for the determination of $\frac{n}{m}$ for each channel in the oxide layer. The width of this layer was chosen as the half–height channel of both the front and back edges of the oxide layer as shown in figure 11. Once the ratio was determined, the prompted input of the value for $N^{Cu_mO_n}_{vol}$ was used to determine the thickness of the oxide layer as defined by the half–height channel values. The ratio versus thickness data for each channel in the layer was output to a text file for each spectrum. See Appendix A for software details.

Text files of the oxide thickness versus exposure time were created for each of the five temperatures. Plots and least square curve fits to these data files were generated using the commercial software Tech*Graph*Pad (Binary Engineering Software, Inc.).

Determination of the Activation Energy and Rate Constant

Once the thicknesses L were determined for several exposure times at a fixed temperature, the data were compared to an equation of the form

$$L(T,t) = \beta^{\frac{1}{2}} e^{-\tau_0/T} t^{\frac{1}{2}} \tag{3.6}$$

where $\beta^{\frac{1}{2}}$ and τ_0 are constants independent of the exposure time and sample temperature. This equation has the same form as that of the theoretical equation 2.53 for the growth of an oxide layer due to uncharged particle diffusion

$$L(T,t) = \left[2\, R\, D_0 \left[C(0) - C(L) \right] \right]^{\frac{1}{2}} t^{\frac{1}{2}} e^{-U/2kT} \tag{3.7}$$

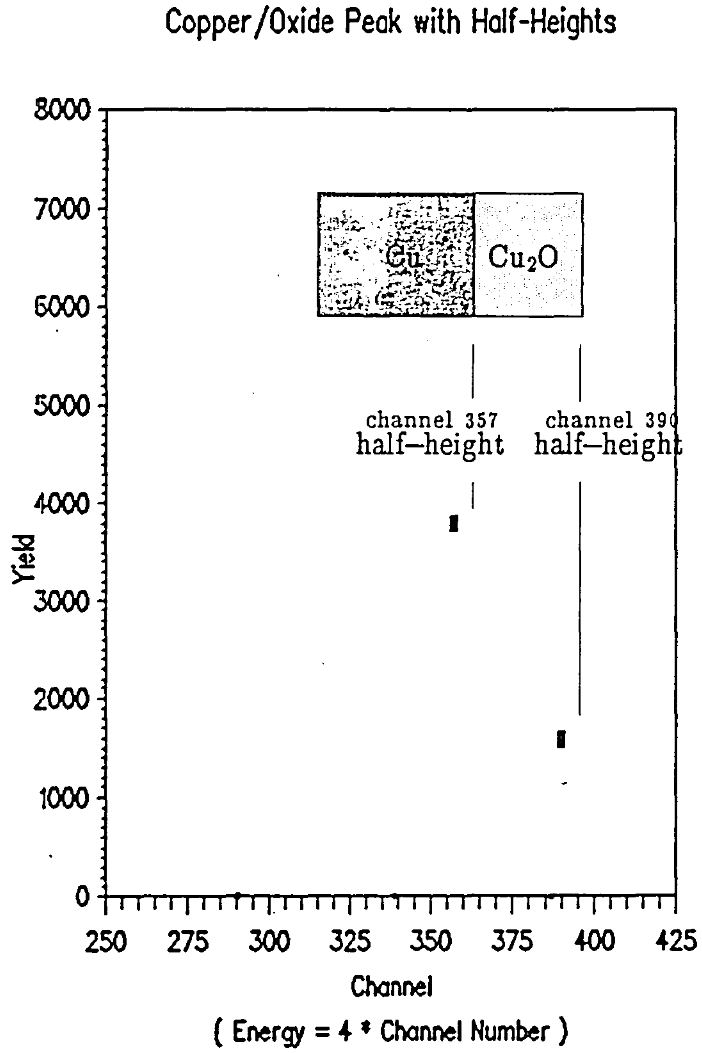

Figure 11. A copper/copper oxide system with an oxide thickness of 1596Å with related spectrum showing the correlation between the front surface oxide, the copper/copper oxide interface, and their respective half–height channel numbers.

when

$$\beta^{\frac{1}{2}} = \left[2\, \mathrm{R}\, \mathrm{D}_0 \left[\mathrm{C}(0) - \mathrm{C}(\mathrm{L}) \right] \right]^{\frac{1}{2}} e^{-\mathrm{U}/\mathrm{kT}}$$

and (3.8)

$$\tau_0 = \mathrm{U}/2\mathrm{k}$$

A section in RESULTS AND CONCLUSIONS, Chapter IV, discusses possible alternative interpretations of the data when considering phenomena such as charged particle diffusion aided by internal electric fields contributing to oxide layer growth.

Activation energy: method one. Linear, natural logarithm and power law curve fits were first performed on these five sets of data to experimentally determine the functional dependence of oxide depth on time. The curve fit equations offering the best correlation to the data were then used to generate fitted values of $L(t_0)$ for fixed values of time t_0 for each of the five temperatures. These fixed times were chosen to represent the entire span of exposure times.

From equation 3.7, the Arrhenius plot of ln(L) for fixed t_0 versus 1/T should be a linear plot of the form $y = mx + b$ with slope m having the value $-U/2k$. A curve fit to each of these linear plots will then yield the activation energy

$$\mathrm{U} = -2\mathrm{mk} \tag{3.9}$$

where m is the slope coefficient of the curve fit, and k is Boltzmann's constant.

Activation energy: method two. Forced quadratic curve fits of L(t) versus $t^{\frac{1}{2}}$ were generated as an alternate method to determine the activation energy for data which is well described by the parabolic growth law. These fits yielded a linear plot with slope m′ where m′ has the value

$$m' = \left[2\,R\,D_o \left[C(0) - C(L)\right]\right]^{\frac{1}{2}} e^{-U/2kT}. \tag{3.10}$$

Determining the value of m′ for each of the five temperature curves yields a set of data relating the slope m′ to the temperature T by the equation

$$\ln(m') = \tfrac{1}{2}\ln\left[2\,R\,D_o \left[C(0) - C(L)\right]\right] - \frac{U}{2kT} \tag{3.11}$$

such that an Arrhenius plot of ln(m′) versus 1/T has slope –U/2k and an intercept

$$b' = \tfrac{1}{2}\ln\left[2\,R\,D_o \left[C(0) - C(L)\right]\right] \tag{3.12}$$

The activation energy can then be assessed using the relation 3.9 and the rate constant β will have the value

$$\beta = e^{b'}. \tag{3.13}$$

combining equation 3.13 and equation 3.12 for uncharged particles the rate constant would be

$$\mathscr{D}_{unch} = R\,D_o \left[C(0) - C(L)\right] = \tfrac{1}{2}\beta^2 \tag{3.14}$$

Error Propagation

Random errors. The error introduced in calculating the oxygen to copper ratio $\frac{n}{m}$ and the oxide depth L due to errors in the parameters used in equations (3.4) and (3.5) can be approximated using the methods outlined by Bevington[17].

For a value Y which is a function of $x_1,x_2,..,x_n$ such that

$$Y = F(x_1,x_2,..,x_n), \tag{3.13}$$

the error ΔY associated with Y can be related to the error Δx_i associated with the independent variables x_i applying the first order approximation[17]

$$\Delta Y^2 \cong \sum_{i=1}^{n} \left[\frac{\partial F(x_i)}{\partial x_i} \cdot \Delta x_i\right]^2. \tag{3.14}$$

where the parameters x_i are assumed to be uncorrelated.

Statistical errors. For a scatter of n data points x_i about some average value $\overline{x}$ defined by

$$\overline{x} = \frac{1}{n} \sum_{i=1}^{n} x_i \tag{3.15}$$

the standard deviation s of the data points is approximated by[17]

$$s^2 = \frac{1}{n-1} \sum_{i=1}^{n} (x_i - \overline{x})^2. \tag{3.16}$$

The error approximations, the average value of the oxide ratios and the standard deviation of this average value for all data taken were calculated using equations (3.14) and (3.16).

IV. RESULTS AND CONCLUSIONS

This chapter contains a discussion of the various results obtained by employing the analytical techniques discussed in Chapter III. Included in the discussion are the establishment of temperature and exposure time ranges over which relevant data could be taken, the measurement of the sample front surface temperature, the oxide phase and layer thickness determination, experimental evaluation of the oxide growth and its functional dependence of time and temperature and the determination of an associated activation energy for the oxide growth resulting from atomic oxygen exposure of copper.

Exposure Range Limitations

Figure 12 is a plot of the oxide thickness versus exposure time curves for five different temperatures between 141°C and 191°C. The following is a discussion of how the particular bounds of exposure time and temperature were determined.

Temperature Limits of Sample Exposures

The temperature range over which timed exposures to atomic oxygen could be produced was limited at the lower end by the RBS depth resolution of approximately 50Å. It was found that for samples exposed for times up to one hour at temperatures below 150°C, the spectra of these samples showed little or no detectable oxide growth, although visual color changes of the sample surface

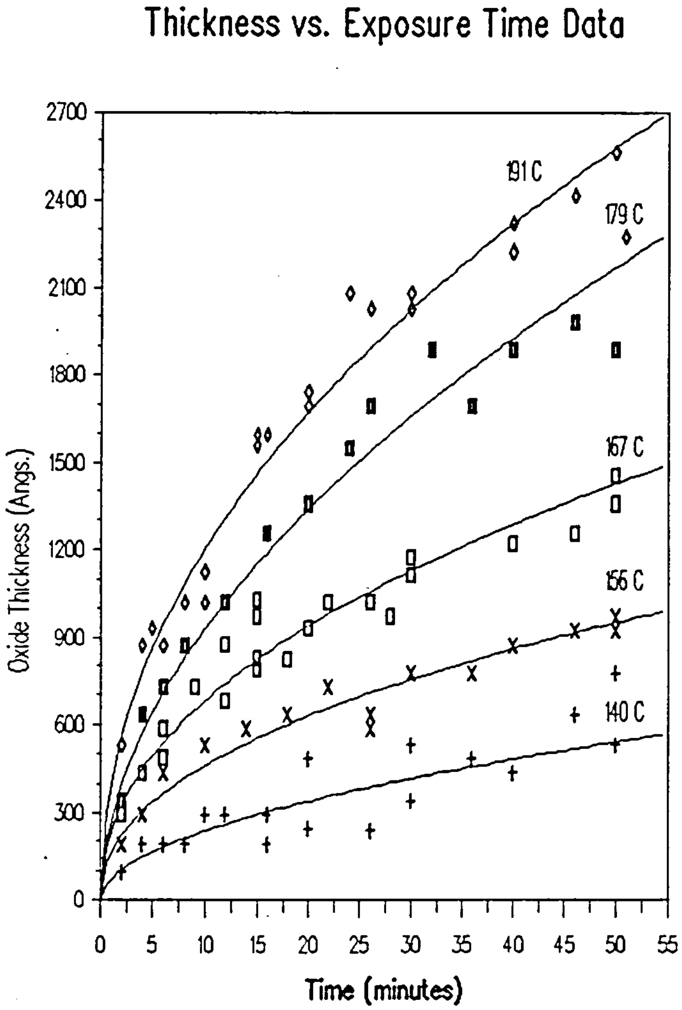

Figure 12. Compilation of all oxide layer thicknesses as a function of exposure time and front surface temperature.

seemed to indicate the occurrence of some oxidation. The heaters in the sample probe (see figure 8) were rated for a maximum temperature of 200°C thus setting the upper bound on the temperature.

The temperature reading from the thermocouple in the probe oscillated about the preset temperature of the controller with a period of approximately 40 seconds – varying about 4°C above and below the setpoint, once equilibrium was established. The maximum and minimum temperatures were recorded for each sample exposure, and the midpoint was used as the probe temperature for that sample. The midpoints were within 2°C of each other for a given setpoint, and the average of all midpoints for a particular temperature curve was the value used for the probe temperature for all samples exposed at a given temperature. These temperatures were 149°C, 162°C, 177°C, 192°C, and 205°C with an error of ±5°C.

Time Limits of Sample Exposures

As with the minimum temperature, the minimum exposure time was limited by the RBS depth resolution. For the lower temperature curves, exposure times of less than 2 minutes produced no detectable oxidation of the sample, thus defining the minimum exposure time.

The upper bound of the exposure times was defined by the appearance of surface deterioration of the oxide layer as the oxidation progressed. For the longer time exposures at 205°C, this deterioration could be observed in the RBS spectra as shown in figure 13. The gradual sloping and broadening of both the back edge of the copper peak and the leading edge of the silicon shoulder is indicative of a roughened surface. As a surface cracks and peals, the angles of the protruding defect areas are not normal to the beam of $^4He^+$ particles so that such an area is

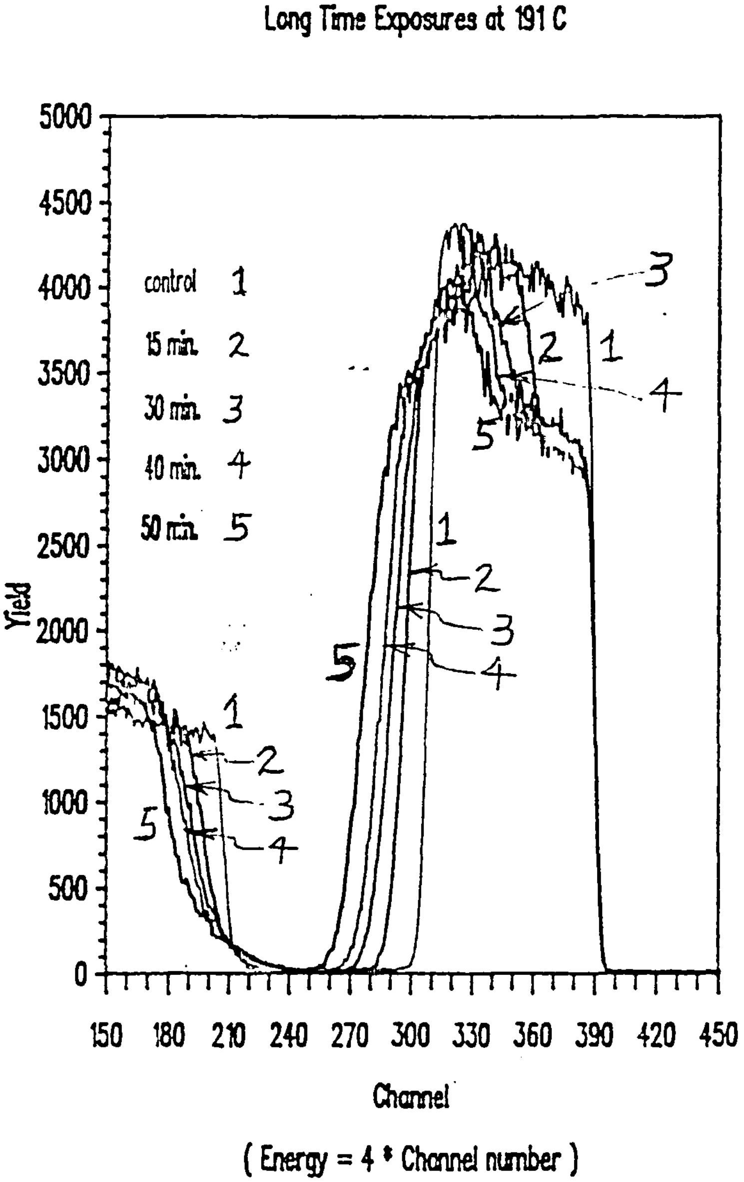

Figure 13. Long exposure copper samples at 191°C showing the broadened, sloping back edge indicating surface damage of the sample.

seen as an effectively thicker surface by the incident particles. Under these conditions, the assumption of a uniform oxide layer breaks down, and accurate thickness determinations cannot be made. In addition, the accuracy of the surface energy approximation (refer to Chapter II) decreases rapidly for thicknesses greater than about 3000Å. To relate this thickness to the spectra of figure 13, the 50 minute exposure has oxide layer approximately 2500Å thick.

The second effect for a damaged surface is to expose parts of the underlying silicon substrate to incident particles which have not lost energy as the result of having traversed the oxide layer. The result is that scattered particle yields from front surface silicon are recorded at higher energies as seen in figure 13. A similar but more pronounced effect has been observed during room temperature oxidation of silver[4].

The scanning electron micrographs in figure 14 were recorded for the samples used to produce the RBS spectra of figure 13. These photographs confirm the presence of roughened surfaces caused by prolonged oxidation. Comparison of the RBS spectra and the SEM photographs also offers an excellent demonstration of the power of Rutherford backscattering for the detection of uniformly distributed surface roughness.

Sample Front Surface Temperature Determination

The probe temperatures discussed in the previous section were measured inside the probe where the thermocouple was in direct contact with the heaters (see figure 8). Tests were performed to determine the ramp time required for the sample to reach a steady state temperature and to investigate the magnitude of any steady state temperature gradient existing across the quartz walls of the probe

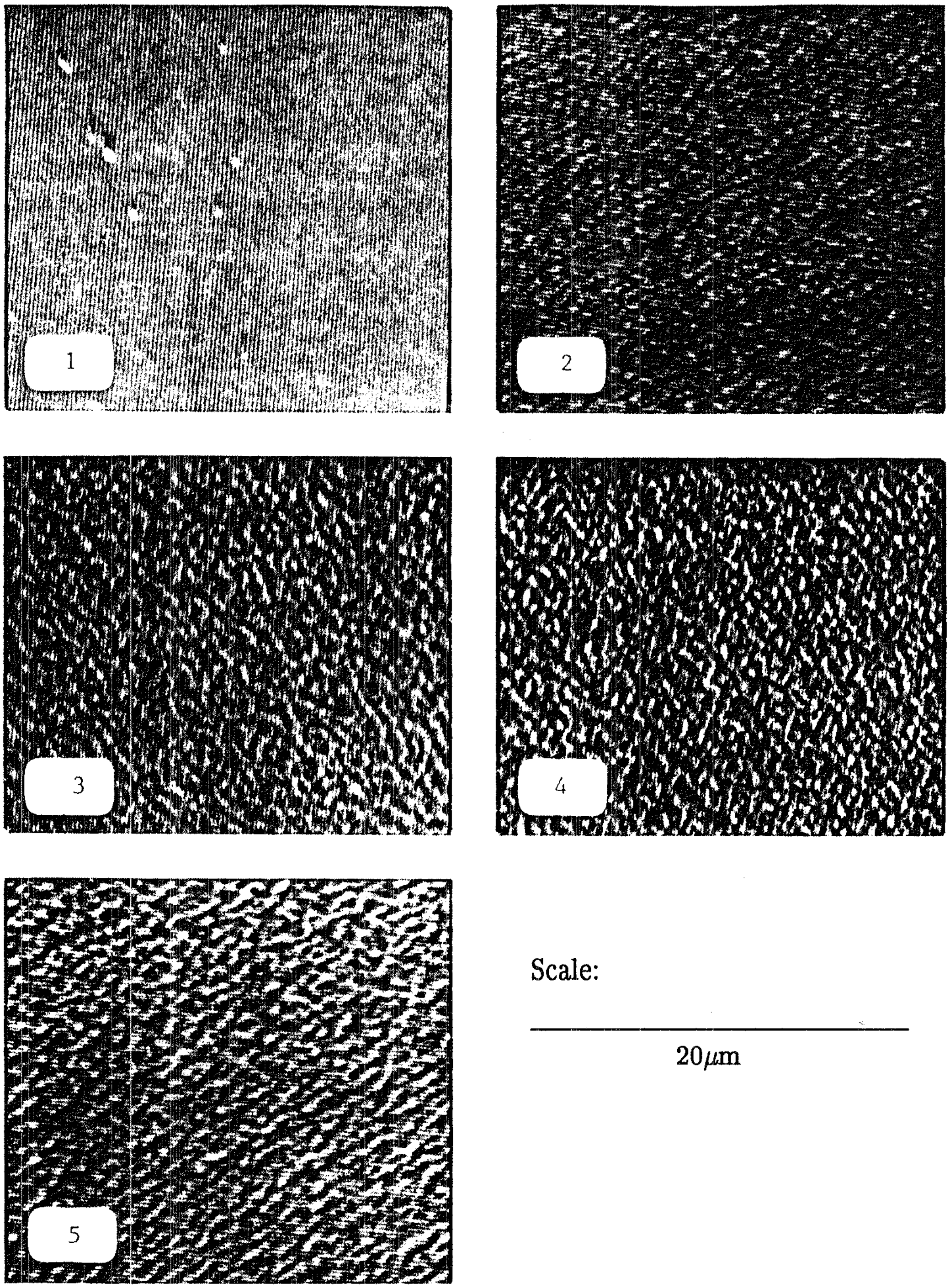

Figure 14. Scanning electron microscope photographs of (1) an unexposed sample and samples exposed at 191°C for (2) 20 minutes, (3) 30 minutes, (4) 40 minutes and (5) 50 minutes to an atomic oxygen flux of 1.4×10^{17} atoms/cm^2–sec.

and the silicon substrate of the sample which together separate the copper film from the heater/thermocouple arrangement inside the probe.

A vacuum chamber flange was equipped with two isolated electrical feedthroughs and an adapter to accommodate the sample probe. The lead and ground wires of a platinum resistance thermometer (PRT) capable of measuring temperatures up to 200°C were soldered to the electrical feedthroughs on the vacuum side of the flange, and the PRT was located at the sample position on the probe. The flange was mounted on the vacuum chamber during the tests, and the chamber was evacuated to a pressure of approximately 0.5 Torr (compared to 1.5 Torr during actual atomic oxygen exposures).

To determine the ramp time of the temperature at the sample surface, the probe was heated to 177°C, and two hours were allowed for the heater unit and the probe temperature to stabilize. A silicon substrate similar in size to those used for the copper exposures was then placed on the probe under vacuum. This took two about minutes, the approximate loading time for sample exposures. The sample surface temperature rose to 166°C after two minutes under vacuum and then began to oscillate about 167° staying within ±2°C of this value. The oscillations occurred at the same frequency as those of the probe, but lagged the oscillations in the probe temperature by about one half of a cycle. The probe temperature setting was set to each of the other setpoints, and steady–state measurements were made for the remaining four probe temperatures of 149°C, 162°C, 192°C, and 205°C. The corresponding steady state sample surface temperatures were 140°C, 156°C, 179°C, and 191°C. No difference in temperature was observed at 25°C.

It was concluded that the minimum time of 10 minutes given each sample to reach thermal equilibrium prior to atomic oxygen exposure (see Experimental Procedure, Chapter III) was more than ample. Also, the existence of steady–state temperature gradients was demonstrated, and the front surface temperature values were adopted as the sample temperatures with assigned errors ±5°C. These temperatures will be the values referred to henceforth in any discussion related to sample temperature. Because the steady–state temperature oscillations were observed using two separate thermometers (the PRT at the sample surface and the thermocouple inside the probe) these oscillations are apparently real – caused by the operation of the heater controller rather than by electronic drift of the temperature readout for the thermocouple inside the probe.

Oxide Phase and Thickness Calculations

Approximately one hundred samples were exposed in the atomic oxygen source once the range limits for temperature and exposure time had been determined. These samples were prepared in eleven separate sets, and the samples were exposed over a span of four months The normal procedure was to expose one group of about eight to ten samples at constant temperature over the full range of the exposure time. Once these data were analyzed and plotted, gaps in the data and questionable data points were assessed More exposures were then made to fill in the gaps and provide additional data for any previously questionable exposure times. Each curve shown in figure 12 consists of exposures made from two to six different occasions.

Rutherford backscattering spectra were taken of each sample exposed to atomic oxygen as discussed in chapter III (EXPERIMENTAL PROCEDURE). Typical spectra over a range of exposure times at 191°C are presented in figure 15. The oxide ratio and thickness were determined for each sample using the computer software documented in appendix A. A typical output file from the software is plotted in figure 16. To relate points on this plot to points on a corresponding

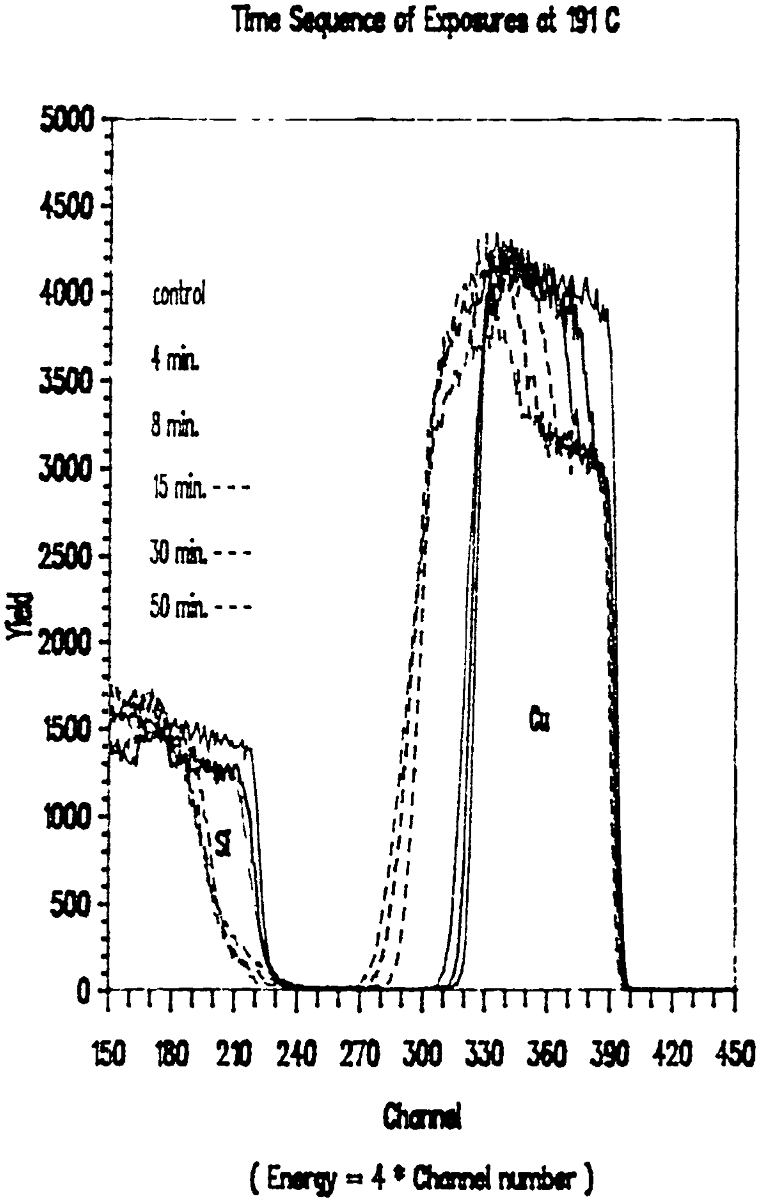

Figure 15. RBS spectra for Cu/Si samples exposed at 191°C for various times.

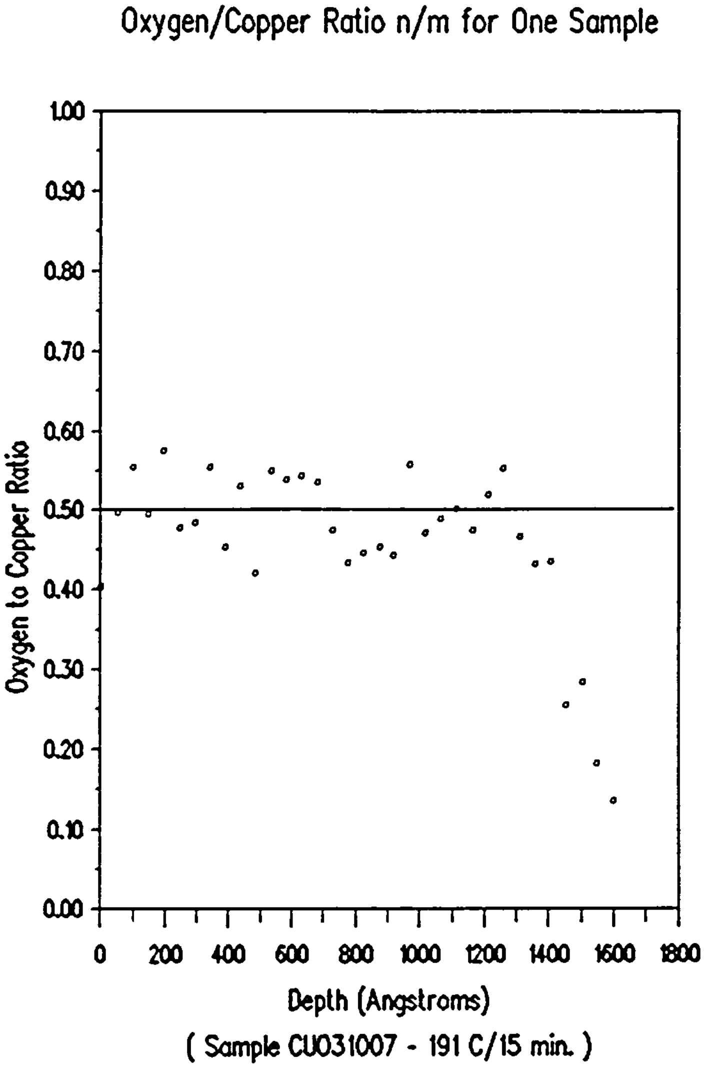

Figure 16. Plotted data from the output file of the analysis program CAMRATV6 for sample CUO31007. The oxygen/copper ratio is plotted versus depth for every channel corresponding to the oxide layer.

RBS spectrum, the oxide ratio at the depth of 0Å corresponds to the O.Cu ratio at the interface half height channel defined in Figure 11, and the ratio at the greatest depth (1595Å in figure 11) corresponds to the half height channel number at the front surface The depth corresponding to this latter channel number is used for the oxide thickness L in later calculations (see figure 5). The average value of the oxide ratio in the oxide layer for each sample comprising the 191°C temperature curve is plotted versus the individual time, as shown in figure 17. To generate this plot, the O/Cu ratio for every channel in the oxide layer is averaged, disregarding the last four points (corresponding to the copper/copper oxide interface) and the first two (corresponding to front surface channels) to avoid erroneous values at the interfaces.

The error associated with the O/Cu ratio n/m was primarily governed by the errors of the peak height values of the control and oxidized sample spectra and by the errors in the alpha particle stopping cross sections The statistical error of the peak heights is approximately the square root of the peak height value, and the stopping cross sections are accurate to approximately 5%[4]. This led to a value of of 0.5 with an absolute error $\Delta(n/m)$ of approximately ±0.1 for the O/Cu ratio in each channel for every spectrum evaluated Errors were propagated using equation (3 11).

The value of $\frac{n}{m} = 0\ 5$ can be predicted to some extent from thermodynamic considerations. The change in free energy of a reaction under specified conditions is equal to the mechanical work done by or absorbed during the process. A simple interpretation of the free energy is that reactions resulting in a loss of free energy are thermodynamically possible and are likely to proceed further toward completion as the change in free energy becomes increasingly negative[19]. The free energies for Cu_c, O_g, and CuO_c at room temperature are[16] 0.0 kJ/mole,

+230.1 kJ/mole and –127.2 kJ/mole respectively such that the free energy of the reaction for

$$Cu + O \rightarrow CuO$$

would be –357.1 kJ/mole. By contrast, the free energy of Cu_2O is –146.5 kJ/mole, and the change in free energy for the reaction

$$2Cu + O \rightarrow Cu_2O$$

is –376.6 kJ/mole. Thus, at room temperature, the oxide phase Cu_2O would be thermodynamically the most probable equilibrium.

From examination of equation (3.4), the error in the calculated ratio due to systematic errors can be assumed to be negligible. Because the values of the peak heights and stopping cross section factors appear as ratios in the equation, any systematic errors in these should tend to cancel.

The error associated with the thickness calculations was determined mainly by the errors assigned to the oxide number density, the energy calibration, the incident beam energy, and the stopping cross sections (5% as previously mentioned). The average oxide density was assigned an error of ±5% of the tabulated value used[16]. The incident energy of 2000 keV was assigned an error of ±20 keV, and the energy calibration for an RBS spectrum was assumed accurate to ±4 keV. This assumption relies on the centroid of the ^{241}Am signal used in the calibration of the energy scale lying no more than one channel to the left or right of the peak channel used to approximate the centroid. With these considerations, the relative error $\Delta L/L$ for thickness L is 12%.

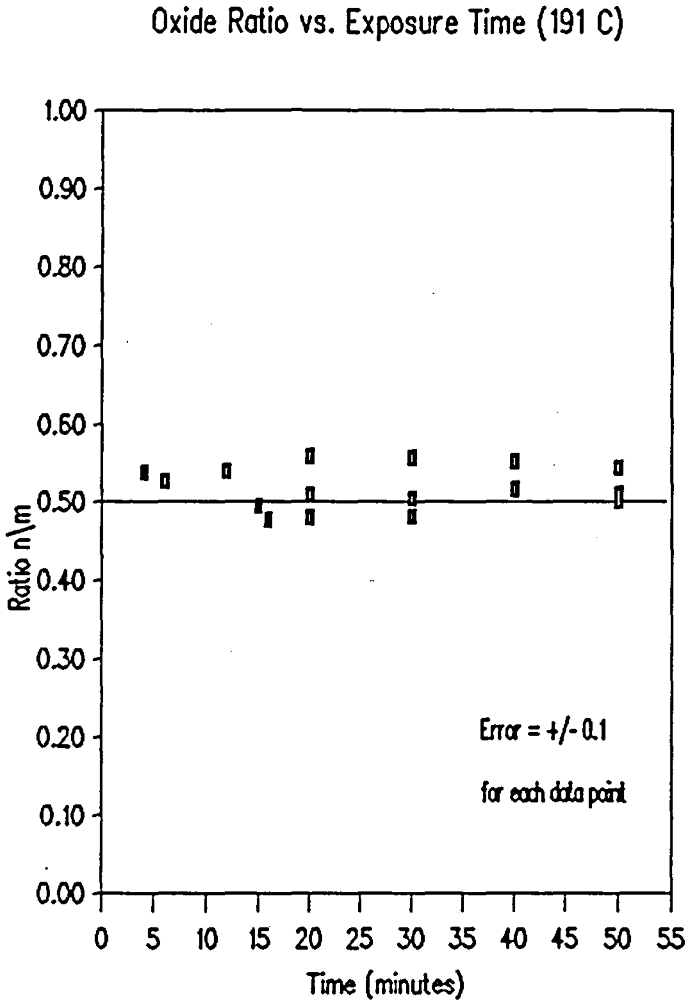

Figure 17. Average O/Cu ratio for 17 of the samples exposed for various times at 191°C.

Some ambiguity also exists regarding which channel of the spectrum is the actual half height channel at the interface or the front surface. An error of ±1 channel was assigned to account for this ambiguity. For the surface energy approximation, there is a linear relationship between channel number and calculated thickness. It was found that each channel represented an oxide increment of 48.4Å. This value was added to the error from the thickness calculation so that the total approximate error for the layer thicknesses L can be taken as

$$\Delta L(\text{Å}) = \pm(50 + 12\%\ L). \tag{4.1}$$

These thickness data are plotted versus exposure times for all temperatures in the figure 12.

The O/Cu ratios and layer thicknesses were also computed using the symmetrical mean energy approximation as a means of checking the validity of the surface energy approximation. The average ratio calculations were found to vary by about 2%. The thickness calculations were equal to within an angstrom for thickness values less than about 500Å. As the thickness of the oxide increased, the SMEA thicknesses were correspondingly smaller than those computed using the SEA. A maximum difference of 42Å occurred at the maximum thickness of 2562Å. The small deviation confirmed that the SEA is an adequate approximation for copper oxide layers less than 3000Å thick, and SEA values for the O/Cu ratio and layer thickness were used for all subsequent calculations.

An RBS spectrum of a 1595Å layer of Cu_2O formed by exposure of a 3000Å copper film on a thick silicon substrate was simulated using the Rutherford Universal Manipulation Program (RUMP)[18]. The parameters describing the simulated spectrum were compared to similar parameters obtained using the analysis program documented in appendix A. Comparison showed excellent agreement in the oxide channel widths (which determine layer thickness) and the oxide layer peak height (which govern the relative atomic concentrations of copper and oxygen). A second simulation was performed of a fictitious sample having the same oxide thickness but with an assumed oxide phase CuO. The oxide shoulder of this spectrum was slightly more narrow, but the most noticeable difference was the drop in the peak height. A plot of the actual spectrum and both simulations is shown in figure 18.

Determination of the Time Dependence of the Oxide Growth

The time dependence of the oxide growth was examined experimentally by fitting different analytical functions to the experimental data using least squares fitting techniques. The coefficients for the linear, natural logarithm and power law curve fits are presented in tables 1, 2, and 3 along with their correlation values. As can be seen, the correlation values for the power law curve fit are consistently higher, having an exponent (b in table 3) with a mean value of 0.48 and a variance of ±0.03. From this, it was concluded that the growth of the copper oxide layer due to ground state atomic oxygen exposure in the temperature range of 140°C to 191°C can well be described by the parabolic growth law. A plot of the 156°C experimental data with the fitted linear, natural logarithm and power law curves are presented in figure 19. A forced parabolic curve fit was applied to the data, and the resulting coefficients are tabulated with the correlation values in table 4 (see page 58) for each of the five temperature curve fits.

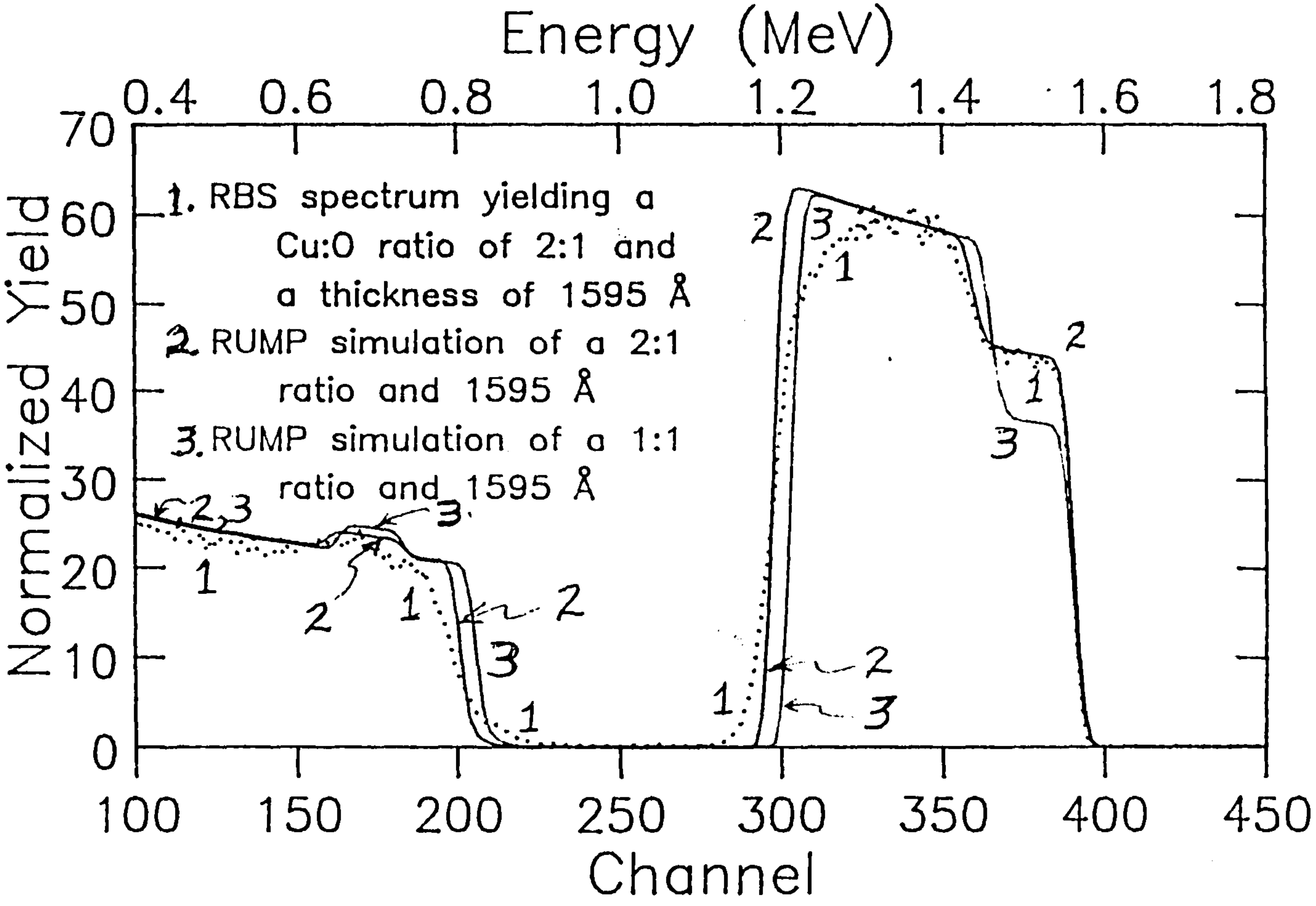

Figure 18. An RBS spectrum of a 1595 Å oxide layer showing the RUMP simulations of Cu_2O oxide phase and CuO oxide phase.

Table 1

Curve Fit Coefficients for the Linear Equation $L(t) = a + bt$ Including the Correlation Factor r

	Temperature				
	140 C	156 C	167 C	179 C	191 C
a	121.296	319.412	506.233	603.538	832.322
b	10.0419	13.2676	18.7639	32.0045	36.4727
r	0.875	0.948	0.940	0.941	0.941

Table 2

Curve Fit Coefficients for the Natural Logarithm Equation $L(t) = a \cdot \ln(bt)$ Including the Correlation Factor r

	Temperature				
	140 C	156 C	167 C	179 C	191 C
a	436.56	245.91	396.42	560.224	691.4482
b	0.127992	0.784535	0.620852	0.668351	0.66177
r	0.373	0.964	0.955	0.982	0.973

Table 3

Curve Fit Coefficients for the Power Law Equation $L(t) = at^b$ Including the Correlation Factor r

	Temperature				
	140 C	156 C	167 C	179 C	191 C
a	73.1737	164.073	164.073	276.344	405.106
b	0.511580	0.448732	0.458226	0.526996	0.473430
r	0.879	0.974	0.972	0.987	0.983

Table 4

Curve Fit Coefficients for the Forced Parabolic Equation $L(t) = at^{\frac{1}{2}}$ (Linear Fit $L(\xi) = a\xi$; $\xi = t^{\frac{1}{2}}$) Including the Correlation Factor r

	Temperature				
	140 C	156 C	167 C	179 C	191 C
a	71.1326	126.804	187.927	293.786	350.107
b	0.500000	0.500000	0.500000	0.500000	0.500000
r	0.690	0.979	0.971	0.985	0.979

Activation Energy Determination

The activation energy U was determined using the curve fit data by the two methods outlined in the Data Analysis section of Chapter III (EXPERIMENTAL PROCEDURE). For method 1, thicknesses L were calculated for each temperature curve for the fixed times of 5, 10, 20, 30, 40 and 50 minutes. An Arrhenius plot of ln(L) versus the inverse Kelvin temperature 1/T was fitted to a linear equation. The activation energy was determined from the slope of this straight line according to equation (3.7). These six plots are shown in figure 20. The activation energy as determined by this method ranged between 1.05eV and 1.06eV.

It should be mentioned at this point that 5 data points were discarded from the data prior to analysis. These data were all on the 191°C curve and were all consistently lower than the remaining data. Furthermore, the samples producing these data points were all exposed during one run on the same day, indicating a probable problem with the gas titration process and a reduced atomic oxygen flux in the source. Equation (2.53) shows theoretically that the oxide thickness L is proportional to the square root of the surface concentration. Thus a reduction in the flux would lead to a drop in concentration and a corresponding drop in oxide thickness. therefore, the points in question were repeated twice each, and the old thickness values were replaced by pairs of new ones.

The value of the activation energy was calculated according to method 1 using all data the points, including the new data points and the questionable points which they replaced. The activation energy obtained using the slopes of the lines generated using all points was typically 3% less than the value of 1.1 eV calculated when disregarding the points in question. This deviation is well within

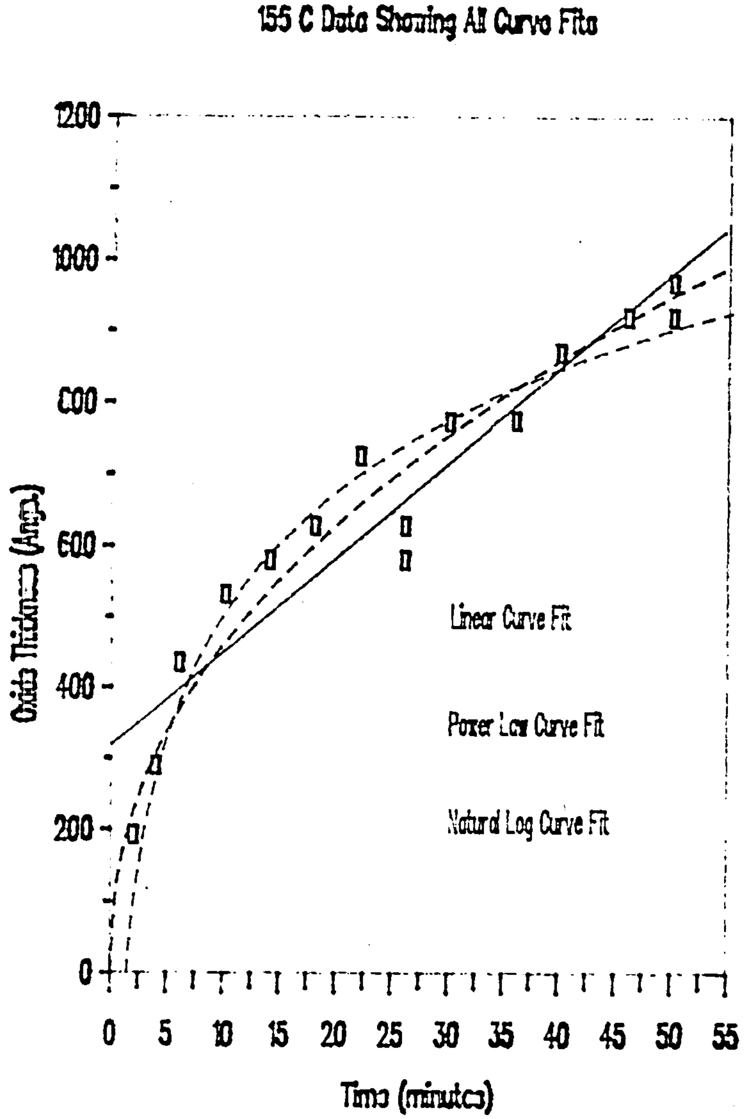

Figure 19. Experimental thickness versus exposure time data for a sample surface temperature of 156°C with fitted linear, power law and natural logarithm curves.

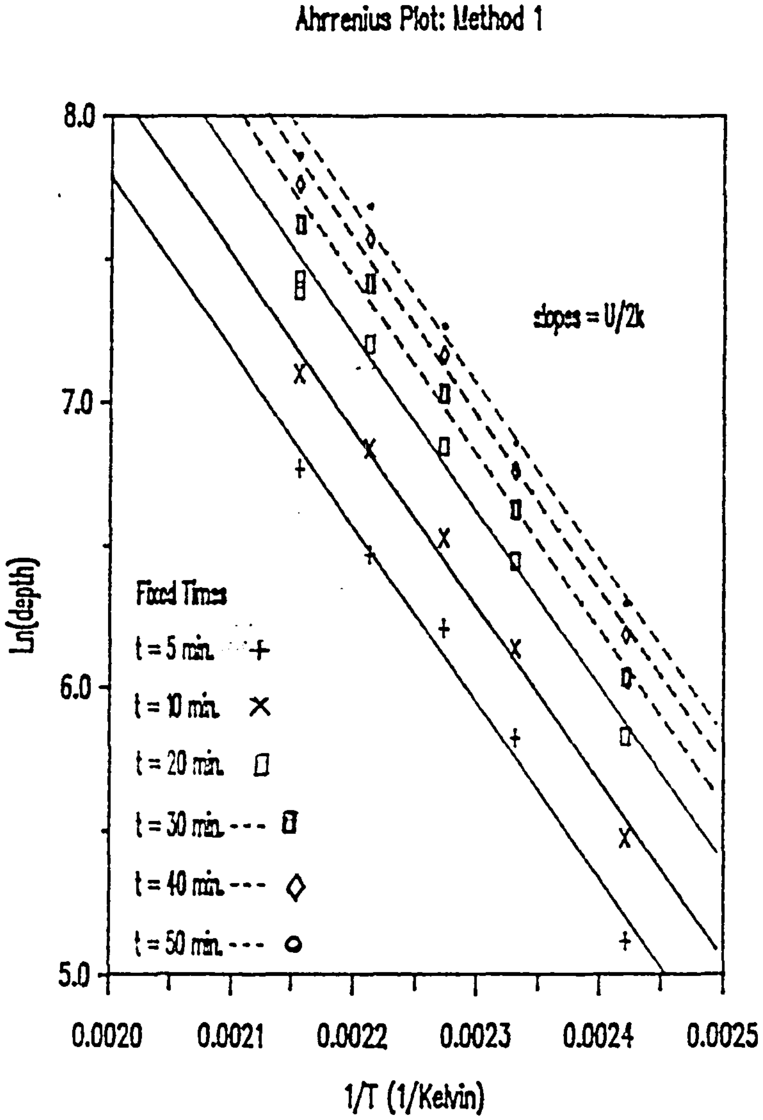

Figure 20. Arrhenius plot of the natural logarithm of the oxide thickness versus the inverse Kelvin temperature, used to determine the activation energy of the copper/atomic oxygen interaction via method 1.

the error associated with the 1.1 eV determination, as will be demonstrated in the following paragraphs.

The forced parabolic fit data of table 4 was next analyzed to determine the activation energy according to method 2 described in the Data Analysis section of Chapter III. An Arrhenius plot of the natural logarithm of the slopes (the coefficient a from table 4) is shown in figure 21 for the five temperatures at which exposures were made. Again, the slope of the line passing through these points is proportional to the activation energy according to equation (3.7), and the resulting value is 1.1eV.

An estimation of the error associated with the activation energy measurements was made by a graphical analysis of the slopes from table 4. A pair of straight line slopes was determined for each of the five data sets corresponding to the five exposure temperatures – one lying just below all points of a data set, and the other lying just above these points. All data were between the two curves for each data set with the restriction that both lines in each pair pass through the origin ($L = 0$, $t = 0$). The deviation of these line slope values from the experimental value for both the upper and lower line slopes were approximately the same and the average deviation of the two was taken to be the uncertainty of the experimental slope.

Arrhenius plots of the natural logarithm of the slopes at maximum deviation and minimum deviation are shown in figure 21. The activation energy corresponding to the maximum and minimum deviation slopes were 0.95 eV and 1.37 eV, respectively.

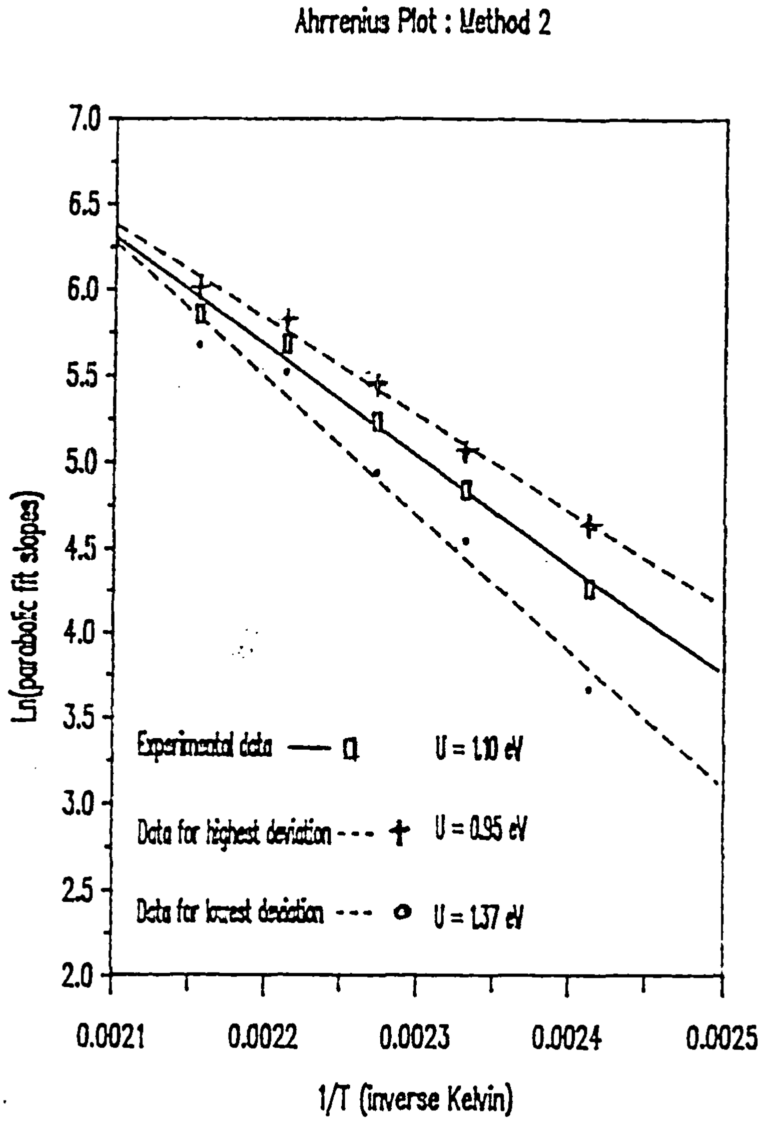

Figure 21. Arrhenius plot used to determine the activation energy of the copper/atomic oxygen interaction via method 2. The dashed lines represent the best line through the data points corresponding to the furthest deviations expected from the experimental data.

The Rate Constant

The rate constant can be determined from the intercept of the line in figure 21. The value $b' = 19.7$ gives a temperature independent rate constant $\mathscr{D}_{\mathrm{unch}} = 6.458\mathrm{x}10^{16}$ Å^2/s where $\beta = 3.594\mathrm{x}10^8$ Å/s$^{\frac{1}{2}}$. Equation 3.6 can now be written in the form

$$\begin{aligned} L(T,t) &= 3.594\mathrm{x}10^8 \exp[-1.1/2kT]\, t^{\frac{1}{2}} \\ &= 3.594\mathrm{x}10^8 \exp[-6373.6/T]\, t^{\frac{1}{2}}. \end{aligned} \tag{4.2}$$

where $L(T,t)$ has units of Å for t in minutes and T in degrees Kelvin. A comparison of the above coefficients of $t^{\frac{1}{2}}$ with those in table 4 is presented in table 5 for each of five temperatures and demonstrates that the curve fit is better at lower temperatures.

Interpretation of the above rate constant varies according to the diffusion mechanism adopted when the data is analyzed. Recall equation 2.58 for uncharged particle diffusion

$$L^2(t) - L^2(t_o) = 2\ \mathscr{D}_{\mathrm{unch}}\, t \tag{4.3}$$

where

$$\mathscr{D}_{\mathrm{unch}} = RD_oe^{-U/kT}[C(0) - C(L)]. \tag{4.4}$$

Equation 4.3 has the same form as the equation used to analyze the data under the assumption that the initial thickness L(0) is approximately zero. Further assuming that the concentration C(0) at the metal–oxide interface is much less than the concentration C(L) at the oxide–oxygen interface, equation (4.3) can be approximated by

Table 5

Comparison of the Coefficients of $t^{\frac{1}{2}}$ as Calculated from Forced Parabolic Curve Fits (see Table 4) and Using the Expression $3.594\text{x}10^{8}(\text{Å}/s^{\frac{1}{2}})\exp(-6373.6/T)$

Temperature	$3.594\text{x}10^{8}e^{-6373.6/T}$ $(\text{Å}/s^{1/2})$	Coefficient a from table 4 $(\text{Å}/s^{1/2})$	Percent Difference
140 C	71.35	71.1326	0.1%
156 C	126.87	126.804	0.05%
167 C	183.93	187.927	1%
179 C	270.20	293.786	8%
191 C	389.10	350.107	10%

$$L(t) \cong \left[-2\ R\ D\ C(L) \right]^{\frac{1}{2}} t^{\frac{1}{2}}. \tag{4.5}$$

where R is negative.

Equation (2.75) developed for the case of uncharged particle diffusion in thin films under the same assumption that $L(0) \cong 0$ can likewise be written

$$L(t) \cong \left[2\ \mathscr{D}_{\text{thin}} \right] t^{\frac{1}{2}} \tag{4.6}$$

where

$$\mathscr{D}_{\text{thin}} \cong 2 \sum_{s=1}^{1} R_s \chi_s, \tag{4.7}$$

$$\chi_s = \mu_s \frac{kT\ln(\eta_0)}{e} \left[\frac{C_s(L) - C_s(0)\exp(Z_s e E_0 L/kT)}{1 - \exp(Z_s e E_0 L/kT)} \right] \tag{4.8}$$

and

$$\ln(\eta_0) = eE_0 L/kT. \tag{4.9}$$

One approximation is to assume the exponential argument $Z_s e E_0 L/kT$ is very small. The exponent can then be approximated by a Taylor series expansion about $E_0 = 0$ and truncated after the first order term

$$\exp[Z_s e E_0 L/kT] \cong 1 + Z_s e E_0 L/kT. \tag{4.10}$$

Substitution of equation 4.10 into 4.8 gives

$$\chi_s = \mu_s \frac{kT\ln(\eta_0)}{e} \left[\frac{C_s(L) - C_s(0)(1 + Z_s e E_0 L/kT)}{1 - (1 + Z_s e E_0 L/kT)} \right]$$

or

$$\beta \cong \mu_s \frac{kT\ln(\eta_0)}{e} \left[\frac{C_s(L) - C_s(0)}{-Z_s e E_0 L/kT} \right].$$

Further substitution of equation 4.9 and

$$\mu_s = \frac{Z_s e D_s}{kT}$$

from the Einstein relation (2.62) gives

$$\chi_s \cong D_s \left[C_s(0) - C_s(L)\right]$$

so that $\mathscr{D}_{thin}$ is now approximated by

$$\mathscr{D}_{thin} \cong \sum_{s=1}^{1} R_s D_s \left[C_s(0) - C_s(L)\right]. \qquad (4.11)$$

For a single diffusant ion of oxygen and a very small electric field in the medium, the rate constant $\mathscr{D}_{thin}$ reduces to that of uncharged particles, $\mathscr{D}_{thin} \cong \mathscr{D}_{unch}$.

This interpretation would, of course, be the expected result as the electric field tends to zero but this tendency is unlikely with charged particle diffusion. For instance, at a temperature of 175°C (representative of the temperature range in this study) $kT \cong 0.04\text{eV}$, and the argument of the exponent (equation 4.10) is

$$\left|\frac{Z_s e E_o L}{kT}\right| = \left|\frac{Z_s e V_o}{kT}\right| \cong 25\ V_o.$$

This would require a potential of $V_o = 0.4\text{mV}$ for an exponential argument of 0.01, whereas the actual potentials are considered to be on the order of a few tenths of a volt, three orders of magnitude higher.

For the case where the exponential argument is large and the electronic mobility μ_2 is much greater than the ionic mobility μ_1, the fluxes of equation 2.67

$$J_s = \mu_s E_o \left[\frac{C_s(L) - C_s(0)\exp(\mu_s E_o L/D_s)}{1 - \exp(\mu_s E_o L/D_s)}\right] \qquad (4.12)$$

can be approximated for metal cation diffusion by

$$J_1 \cong \mu_1 E_0 C_1(0) \tag{4.13}$$

and

$$J_2 \cong 0. \tag{4.14}$$

Substitution of 4.14 into 4.12 and solving for E_0 gives

$$E_0 = \frac{1}{L}\frac{D_2}{\mu_2}\ln\left[\frac{C_2(L)}{C_2(0)}\right], \tag{4.15}$$

and substitution of this expression into equation 4.13 gives

$$J_1 \cong \frac{1}{L}\frac{\mu_1}{\mu_2} D_2 \ln\left[\frac{C_2(L)}{C_2(0)}\right] C_1(0).$$

Using the Einstein relation, J_1 can be written

$$J_1 \cong \frac{1}{L}\frac{kT}{Z_2 e} D_1 C_1(0) \ln\left[\frac{C_2(L)}{C_2(0)}\right] \tag{4.16}$$

so that the solution of $dL/dt = R_1 J_1$ is parabolic with a rate constant

$$\mathscr{A}_{\mathrm{thin}} \cong R_1 D_1 C_1(0) \frac{kT}{Z_2 e} \ln\left[\frac{C_2(L)}{C_2(0)}\right]. \tag{4.17}$$

Here, Z_2 is negative so that R_1 and the logarithm would have the same sign, giving an overall positive value consistent with theory.

Similar analysis for oxygen anion diffusion would give a flux J_1 approximated by

$$J_1 \cong \frac{1}{L} D_1 C_1(L) \frac{kT}{Z_2 e} \ln\left[\frac{C_2(L)}{C_2(0)}\right], \tag{4.18}$$

and the corresponding rate constant would be

$$\mathscr{A}_{thin} \cong R_1D_1C_1(L)\frac{kT}{Z_2e}\ln\left[\frac{C_2(L)}{C_2(0)}\right] \tag{4.19}$$

where R_1 has the same sign as the logarithm for a positive rate constant. The experimentally determined rate constant could then be interpreted under these conditions as the rate constant of equation 4.19. Furthermore, if both cation and anion diffusion are occurring, the rate constant would be described by the sum of equations 4.17 and 4.19.

For the growth of a thick oxide layer due to charged particle diffusion, a region of space charge neutrality should eventually become large enough that the growth of a layer with thickness greater than $L(t_o)$ is well described by Fromhold's thick oxide growth law[13]. Then

$$L^2(t) - L^2(t_o) = 2\mathscr{A}_{thk}(t - t_o) \tag{4.20}$$

where

$$\mathscr{A}_{thk} = R_1\left[\frac{\mu_1D_2-\mu_2D_1}{\mu_1-\mu_2}\right][C_1(\delta^*)-C_1(L^*)], \tag{4.21}$$

and the concentrations $C_1(\delta^*)$ and $C_1(L^*)$ are given by equations 2.91 and 2.92. Upon substitution of equation 2.62, equation 4.21 can be written

$$\mathscr{A}_{thk} = R_1\left[\frac{(Z_1 - Z_2)D_2}{Z_1 - Z_2(D_2/D_1)}\right][C_1(\delta^*)-C_1(L^*)]. \tag{4.22}$$

Assuming that the electronic diffusion coefficient is much greater than the coefficient of the ion species, equation 4.22 becomes

$$\mathscr{A}_{thk} = R_1D_1\left[\frac{Z_2 - Z_1}{Z_2}\right][C_1(\delta^*)-C_1(L^*)]. \tag{4.23}$$

Further assumption that $C_1(L^*) >> C_1(\delta^*)$ for a oxygen anion diffusant where $Z_2={}^{+}1$, the rate constant can be approximated

$$\mathscr{D}_{hk} \cong R_1D_1(1-Z_1)C_1(L)\left[\frac{Z_1C_1(0)}{-C_2(0)}\right]^{-Z_1/(Z_1-1)} \tag{4.24}$$

where $C(\delta^*)$ has been expressed using equation 2.91. Comparison to equation 4.5 where a similar assumption that $C(L) >> C(0)$ for anion diffusants reveals

$$\mathscr{D}_{hk} \cong (1-Z_1)\left[\frac{Z_1C_1(0)}{-C_2(0)}\right]^{-Z_1/(Z_1-1)} \mathscr{D}_{unch} \tag{4.25}$$

where $\mathscr{D}_{hk}$ is again positive, as required.

The purpose of these approximations is to demonstrate that, depending on the mechanism of diffusion chosen, interpretation of the rate constant for the determination of quantities such as diffusion coefficients or surface concentrations will be different. For example, equation 4.25 shows that for singly ionized oxygen diffusion in a thick oxide layer, the diffusion coefficient values could differ by a factor of

$$(1-Z_1)\left[\frac{Z_1C_1(0)}{-C_2(0)}\right]^{-Z_1/(Z_1-1)} = 2\left[\frac{C_1(0)}{C_2(0)}\right]^{-\frac{1}{2}}$$

compared to uncharged particle diffusion in a thick layer. This difference may be several orders of magnitude.

Summary

A study of the interaction of atomic oxygen with thin evaporated copper films was performed for controlled exposure times and temperatures using the atomic oxygen source located in the Space Power Institute at Auburn University. An atomic oxygen flux of 1.4×10^{17} atoms/cm^2–sec was generated by the titration of NO with N atoms produced by the microwave dissociation of N_2

Rutherford backscattering spectroscopy was the primary analytical technique employed to investigate the resulting copper oxide layers which formed on the copper surface. The Rutherford backscattering facility is equipped with a sample holder which accommodates up to twelve samples for one experiment. Both the sample holder and a surrounding shield were biased to minimize beam current losses during data acquisition.

The O/Cu ratio in the oxide layers of all exposed samples was found to be 0.5 ± 0.1 – indicating that the oxide phase Cu_2O was the predominant phase formed during exposures over the temperature range of 140°C to 191°C. The phase Cu_2O was the only phase detected in the RBS analysis. Over this temperature range, the growth of the oxide layer can be reasonably well described by a parabolic growth law with respect to time and temperature. For linear, logarithmic and power law curve fits, oxide layer growth correlated most strongly to a power law dependence on exposure time. For five different exposure temperatures (140°C, 156°C, 167°C, 179°C, and 191°C), the power of the time dependence ranged from 0.44 to 0.53 with an average value of 0.48. This value is within 4% of the theoretical value 0.5 for a parabolic growth law.

The growth process for the oxide layers also exhibits an Arrhenius temperature dependence with an activation energy lying between 1.0eV and 1.4eV and having a most probable value of 1.1eV. The published value of 1.7 eV for the diffusion of diatomic oxygen through Cu_2O is consistent with this result in that it is higher than the value 1.1 eV determined in this study for the diffusion of monatomic oxygen[20]. The temperature dependent rate constant for the growth of an oxide layer was found to be 6.458×10^{16} Å^2/s exp[−1.1eV/kT].

Rutherford backscattering spectra showed some indication of surface damage for the longer exposure/higher temperature samples. Scanning electron microscopy confirmed this indication and gave some insight as to the minimum amount of damage detectable using Rutherford backscattering methods.

REFERENCES

1. D. L. Edwards, M.S. Thesis, Auburn University (1989)
2. P. N. Peters, J. C. Gregory, J. T. Swann, Applied Optics, **4** 1290 (1985)
3. P.N. Peters, R. C. Linton, E. R. Miller, Geophysical Review Letters, **10(7)** 569 (1983)
4. W. K. Chu, J. W. Mayer and M. A. Nicolet, Backscattering Spectrometry (Academic Press, New York, 1978)
5. H. Goldstein, Classical Mechanics, 2nd ed. (Addison–Wesley, Reading, Massachusetts, 1980)
6. J. F. Zeigler, Helium: Stopping Powers and Ranges in all Elemental Matter (Pergammon Press, New York, 1977)
7. P. Shewmon, Diffusion in Solids, 2nd ed. (The Minerals, Metals and Materials Society, Pennsylvania, 1989)
8. Richard Ghez, A Primer of Diffusion Problems, (Wiley, New York, 1988)
9. Private communication, A. T. Fromhold
10. A. T. Fromhold, Journal of Chemical Physics, **41(2)** 509 (1964)
11. A. T. Fromhold, Journal of Chemistry and Physics of Solids, **33** 95 (1972)
12, A. T. Fromhold, Physics Letters, **58A(2)** 118 (1976)
13. A. T. Fromhold, Journal of the Physical Society of Japan, **48(6)** 2022 (980)
14. P. K. Van Staagen, M.S. Thesis, Auburn University (1989)
15. R. G. Musket and S. W. Taatjas, Review of Scientific Instruments, **44(9)** 1290 (1973)
16. R. C. Weast, Handbook of Chemistry and Physics, 61st ed. (CRC Press, Florida, 1981)
17. P. R. Bevington, Data Reduction and Error Analysis for the Physical Sciences (McGraw–Hill, New York, 1969)

18. L. Doolittle, Ph.D. Dissertation, Cornell University (1985)

19. C. E. Wicks and F. E. Block, Thermodynamics Properties of 65 Elements – Their Oxides, Halides, Carbides, and Nitrides, U.S. Bureau of Mines, Washington, 1963)

20. O. Kubaschewski and B. E. Hopkins, Oxidation of Metals and Alloys, 2nd ed. (Butterworths, London, 1962)

APPENDIX

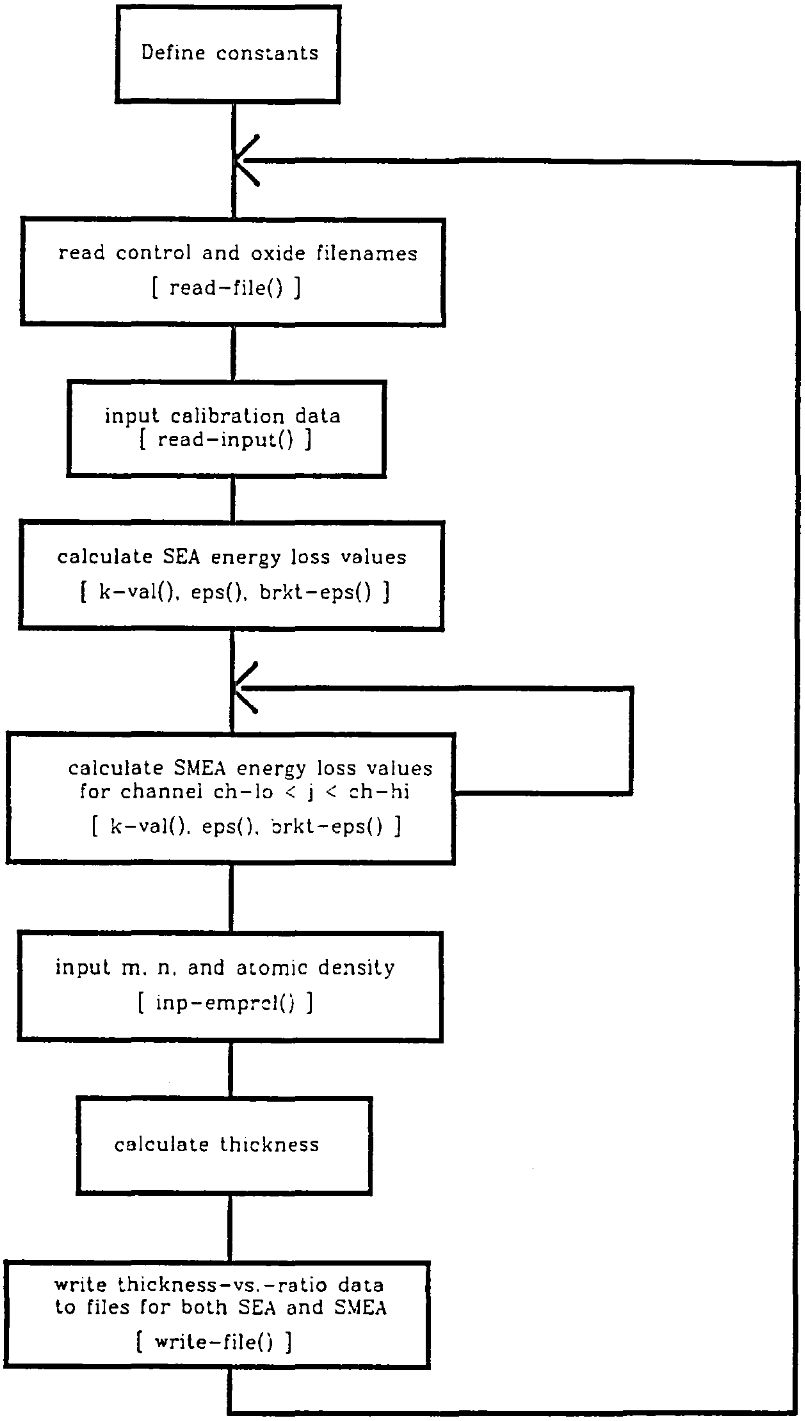

Figure 22. Software flowchart of the program "CAMRATV6.C".

****

This is the documented version of the C program "CAMRATV6.C". Text not appearing in the actual C file will be set between rows of asterisks just as this paragraph is. The basic functions of the program are to (1) read two files corresponding to the spectra of a sample before and after exposure, (2) prompt the user for calibration parameters and the beginning and ending channels corresponding to the oxide layer window, (4) determine the ratio of copper to oxygen and the depth into the sample corresponding to each channel in the user defined window with depths calculated using both the surface energy approximation (SEA) and the symmetrical mean energy approximation (SMEA), and (5) store the data for both approximations in text files.

****

****

The include statements below initialte the libraries of the library directories in the commercial software packages TURBOC2 and GREENLEAF.

****

```
#include <gf.h>
#include <ibmkeys.h>
#include <asiports.h>
#include <math.h>
#include <stdio.h>
#include <stdlib.h>
#include <string.h>
```

****

The statements below define the user–written funtions used in the program.

****

```
void write_file();
void read_file();
void read_input();
double k_val();
double eps();
double brkt_eps();
double inp_emprcl();
```

****

These statements define the external variables accessible to all functions in the program. They contain the following parameters:

H[3][512] is a 3x512 matrix containg peak heights(counts) for the 512 channel wide spectra of the copper and copper oxide spectra.

m[3] is a one dimensional array containing the masses of the alpha particle, e oxygen nucleus and the copper nucleus

a[3][6] is a 3x6 array containing the coefficients of the polynomial curve fit for the stopping cross section ε^{777}.

hi_ch and lo_ch are the respective variables for the user input high and low channels of the oxide window.

con0,con1 and con2 are the user input coefficients for the

```
        channels–to–energy calibrated curve fit.
    sea_rat[512], smea_rat[512], thk_sea[200] and thk_smea[200] are the
        calculated ratios and thicknesses for each channel in the oxide
        window for the SEA and SMEA approximations
    sbrak_eps[3] is a one dimensional array containg the stopping cross section
        factor for the different target atoms using the SEA approximation.
    mbrak_eps[3][512] is a 3x512 array containing the stopping cross section
        factor at each channel using the SMEA approximation
    outfile[30] is a character array containg user input file names for
        input/output operations
**********************************************************************

double H[3][512];
double m[3];
double a[3][6];
double hi_ch,lo_ch,con0,con1,con2;
double sea_rat[512],smea_rat[512],thk_sea[200],thk_mea[200];
double sbrak_eps[3];
double mbrak_eps[3][512];
char outfile[30];

**********************************************************************
The variables defined below are for the temporary storage default values of
user–input information.
**********************************************************************

char def_hi[20],def_lo[20],def_a[20],def_b[20],def_c[20];
char defstr[3][25],def_app[25];
char def_emp[3][25];

**********************************************************************
The following are user defined constants of the incident beam energy E0, pi, the
backscattering angle theta, and the array pointers ALPHA, O and Cu for the
respective alpha particle, oxygen, and copper.
**********************************************************************

#define E0 2000.0      /* incident beam energy (keV) */
#define pi 3.1415962
#define theta 164.0*(pi/180.0) /* beam scattering angle (degrees) */
#define ALPHA 0
#define O 1
#define Cu 2

**********************************************************************
main contains the controlling body of the program from which all user– and
commercially written functions are called.  All user–written functions will be
described in detail at their respective locations following the main program.
Predefined external variables will not be redefined.
**********************************************************************
```

```
main()
{
extern double H[][];
extern double m[];
extern double a[][];
extern double hi_ch,lo_ch,con0,con1,con2;
extern double sea_rat[];
extern double smea_rat[];
extern char def_hi[],def_lo[],def_a[],def_b[],def_c[];
extern char defstr[][],def_app[];
extern char def_emp[][];
extern double sbrak_eps[],mbrak_eps[][];
double mrat,srat;
extern double thk_sea[],thk_mea[];
extern char outfile[];

************************************************************************
These declared variables are local to main and contain the values as follows:
        eps_in and eps_out contain the values as calculated by the function eps()
                and correspond to the values ε(Ein) and ε(Eout) of Chapter II.
        K[3] is an array of the kinematic factors for the target atoms.
        E1[512], Ein and Eout correspond to E1, Ein and Eout of chapter II.
        emp_m and emp_n are the user input values of m and n assessed from the
                ratio determination.
        density is the user input density of the oxide assumed from determining the
                oxide phase.
        deltaE has the value of ΔE of Chapter II.
        i is a general purpose counter, normally used for channel numbers
        shft[5] contains the user input difference between the FWHM front surface
                values between the unoxidized and oxidized spectra.
        flptr is a file address specifier locating the pointer position in an i/o file
************************************************************************

double eps_in,eps_out;
double K[3],E1[512],Ein,Eout;   /* kinematic factors */
double emp_n,emp_m,density,deltaE;
int i;
char shft[5];
unsigned key;
int shift;
FILE *flptr;

************************************************************************
Values are initialized here for defaults and specific target atoms
************************************************************************

def_hi[0]='\x0';
def_lo[0]='\x0';
def_a[0]='\x0';
def_b[0]='\x0';
def_c[0]='\x0';
```

```
defstr[0][0]='\X0';
defstr[1][0]='\x0';
defstr[2][0]='\x0';
def_app[0]='\x0';
def_emp[0][0]='\x0';
def_emp[1][0]='\x0';
def_emp[2][0]='\x0';

a[O][0]=25.9;
a[O][1]=73.3;
a[O][2]=–80.5;
a[O][3]=35.17;
a[O][4]=–7.1;
a[O][5]=0.5462;

a[Cu][0]=40.72;
a[Cu][1]=73.99;
a[Cu][2]=–56.66;
a[Cu][3]=18.06;
a[Cu][4]=–2.656;
a[Cu][5]=0.1452;

m[0]=4.002603; /* incident particle a.m.u.(He) */
m[O]=15.994915*0.9976+16.999133*0.0004; /*oxygen a.m.u. */
m[Cu]=62.929592*0.6917+64.927786*0.3083; /* Cu a.m.u.   */
```

```
***********************************************************************
```

Here the user–written function read_file() reads the data files for the sample under analysis. The flag morefiles is referenced should the user opt not to store oxide ratio data for these sample files.

```
***********************************************************************
```

```
morefiles:
read_file(Cu,"control");
read_file(O," oxide ");
```

```
***********************************************************************
```

The user–written function read_input() prompts the user for calibration data and oxide window channel numbers. The user then inputs the number of channels to shift the unoxidized spectrum so front surface FWHM values match.

```
***********************************************************************
```

```
read_input();
puts("shift control spectrum by:");
shift=atoi(gets(shft));
```

****
Energy loss parameters are determined using the user written functions and the oxide ratio-per-channel calculations are made and stored in the proper arrays. These calculations are in accordance with those discussed in chapters II and III for the SEA and SMEA approximations.
****

```
K[Cu]=k_val(Cu,theta);

for(i=hi_ch;i>=lo_ch;--i){

eps_in=eps(Cu,E0);
eps_out=eps(Cu,K[Cu]*E0);
sbrak_eps[Cu]=brkt_eps(K[Cu],theta,eps_in,eps_out);

eps_in=eps(O,E0);
eps_out=eps(O,K[Cu]*E0);
sbrak_eps[O]=brkt_eps(K[Cu],theta,eps_in,eps_out);

sea_rat[hi_ch-i]=((H[Cu][i+shift]/H[O][i]-1)*sbrak_eps[Cu]/
        sbrak_eps[O]);

E1[i]=con0+con1*i+con2*i*i;
Ein=E0-(K[Cu]*E0-E1[i])/4.0;

eps_in=eps(Cu,Ein);
eps_out=eps(Cu,Eout);
mbrak_eps[Cu][i]=brkt_eps(K[Cu],theta,eps_in,eps_out);

eps_in=eps(O,Ein);
eps_out=eps(O,Eout);
mbrak_eps[O][i]=brkt_eps(K[Cu],theta,eps_in,eps_out);

smea_rat[hi_ch-i]=(H[Cu][i+shift]/H[O][i]-1)*mbrak_eps[Cu][i]/
        mbrak_eps[O][i];
}
```

****
The average values for the ratios using the SEA (srat) and SMEA (mrat) are calculated and the user is queried whether to continue or not. If the answer is no (N) control is moved to the flag morefiles.
****

```
srat=0;
mrat=0;

for(i=1;i<=hi_ch-lo_ch-1;++i){
srat+=sea_rat[i];
mrat+=smea_rat[i];
}
```

```
srat=srat/(hi_ch-lo_ch-1);
mrat=mrat/(hi_ch-lo_ch-1);

printf("\n\n");
printf("average ratio for SEA approximation is\n%g\n",srat);
printf("average ratio for SMEA approximation is\n%g\n",mrat);

getagain:
puts("");
puts("");
puts("PROCEDE?");
do{}while(gfkbhit()==FALSE);
key=toupper(getkey());

switch(key){
default: goto getagain;
case 'N': goto morefiles;
case 'Y': break;
}

**********************************************************************
User input values of m and n and the density of the assumed oxide are input here.
**********************************************************************

emp_m=inp_emprcl("# atoms Cu",2);
emp_n=inp_emprcl("# atoms O",1);
density=inp_emprcl("# density (atoms/cm^3)",0);

**********************************************************************
The depth corresponding to each channel of the oxide window is calculated here for
both SEA (thk_sea) and SMEA (thk_smea).
**********************************************************************

for(i=hi_ch;i>=lo_ch;--i){
deltaE=(K[Cu]*E0-E1[i])*1000; /* deltaE (keV) */

thk_sea[hi_ch-i]=deltaE/(density*(emp_m*sbrak_eps[Cu]
        +emp_n*sbrak_eps[O]));

thk_sea[hi_ch-i]*=1e8;  /* thickness in angstroms */

thk_mea[hi_ch-i]=deltaE/(density*(emp_m*mbrak_eps[Cu][i]
        +emp_n*mbrak_eps[O][i]));
thk_mea[hi_ch-i]*=1e8;
}
```

```
************************************************************************
User is prompted to name the files for data storage of thickness vs. oxide
calculations, after which program control returns to the flag morefiles
************************************************************************

write_file("SEA data","A:SEA\\flname.DAT\n");

flptr=fopen(outfile,"wt");
for(i=0;i<=hi_ch-lo_ch;++i)
fprintf(flptr,"%g %g\n",(thk_sea[i]-thk_sea[0]),sea_rat[i]);
fclose(flptr);

write_file("SMEA","A:SMEA\\flname.DAT\n");
flptr=fopen(outfile,"wt");
for(i=0;i<=hi_ch-lo_ch;++i)
fprintf(flptr,"%g %g\n",(thk_mea[i]-thk_mea[0]),smea_rat[i]);
fclose(flptr);

goto morefiles;
}

************************************************************************
USER-WRITTEN FUNCTIONS
************************************************************************

************************************************************************
The function read_file() reads a type = Cu/tp_str = "control" or
type = O/type_str = "oxide" file name, checks that the file exists, and loads the
second column of data in the file into the H[][] array.
************************************************************************

void read_file(type,tp_str)
int type;
char tp_str[25];
{
extern double H[][];
extern char defstr[][];

************************************************************************
The variable file_name[3][25] contains the input control and oxide text file names,
j is a counter, and string[] is a temporary string for the text file data.  The
filepointer fp points to the current address of the current input file.
************************************************************************

char file_name[3][25];
unsigned long int j;         /* counter */
char string[25]; /* dummy string for text data */
FILE *fp;
```

```
************************************************************************
Set the flag control and initialize filenames to NULL
************************************************************************

control:
file_name[0][0]=’\x0’;
file_name[type][0]=’\x0’;

************************************************************************
Prompt user for a file name and update the default filename.
************************************************************************

printf("Enter %s spectrum txt_file name(def %s): ",tp_str,defstr[type]);
gets(file_name[type]);
if(file_name[type][0]==’\x0’)
strcpy(file_name[type],defstr[type]);
else
strcpy(defstr[type],file_name[type]);

************************************************************************
Check that the file exists at the specified path.
************************************************************************

if((fp=fopen(file_name[type],"rt"))==NULL){
printf("FILE NOT ON DISK! TRY AGAIN\n");
fclose(fp);
goto control;
}

************************************************************************
Fill the array H[][] with the data, disregarding all data points having a the value 0
in the first column. (Some of the text files to be read contained an erroneous first
and sometimes second pair of data points with a channel number of 0 in the first
column.)
************************************************************************

for(j=1;!feof(fp);++j){
fscanf(fp,"%s",string);
if(atof(string)==0){
fscanf(fp,"%s",string);
fscanf(fp,"%s",string);
}

fscanf(fp,"%s",string);
H[type][j]=atof(string);
}
}
```

```
***********************************************************************
The function k_val() determines the kinematic factor for type = Cu or type = O
and at an angle = angle
***********************************************************************

double k_val(type,angle)
double angle;
{

***********************************************************************
The variable beta is the projectile–to–target mass ratio, root is a temporary
variable, and k is the kinatic factor passed back to main().
***********************************************************************

double beta;
double root;
double k;

beta=m[0]/m[type];
root=sqrt(1–pow(beta*sin(angle),2));
k=pow((root+beta*cos(angle))/(1+beta),2);
return(k);
}

***********************************************************************
The read_input() function prompts the user to input the calibration data,
correction factors and shift of the control spectrum, and updates the default
values. The variable buff[25] is a temporary array for the user–input data.
***********************************************************************

void read_input()

{
char buff[20];
extern char def_hi[],def_lo[],def_a[],def_b[],def_c[];
extern double con0,con1,con2,hi_ch,lo_ch;

***********************************************************************
User is prompted to input front surface channel number. For a NULL input,
program control is passed to the flag frntsfc. Otherwise, the value is assigned and
the default is updated.
***********************************************************************

frntsfc:
buff[0]='\x0';
printf("Enter front surface channel number(def %s): ",def_hi);
gets(buff);
```

```
if(buff[0]!=’\x0’){
hi_ch=atof(buff);
strcpy(def_hi,buff);
}
else {
hi_ch=atof(def_hi);
}

************************************************************************
User is prompted to input back surface channel number.  For a NULL input,
program control is passed to the flag bcksrfc.  Otherwise, the value is assigned and
the default is reset.
************************************************************************


bcksrfc:
buff[0]=’\x0’;
printf("Enter back surface channel number(def %s):  ",def_lo);
gets(buff);

if(buff[0]!=’\x0’){
lo_ch=atof(buff);
strcpy(def_lo,buff);
}
else {
lo_ch=atof(def_lo);
}

************************************************************************
User is prompted to input the three calibration coefficients corresponding to those
of the second order curve fit equation.  Defaults are reset upon entry of the data.
************************************************************************


puts("\nCORRECTION FACTORS");
puts("E = a + b(ch#) + c(ch#)^2");

inp_con0:
buff[0]=’\x0’;
printf("Enter a–value(def %s):  ",def_a);
gets(buff);

if(buff[0]!=’\x0’){
con0=atof(buff);
strcpy(def_a,buff);
}
else {
con0=atof(def_a);
}
inp_con1:
buff[0]=’\x0’;
printf("Enter b–value(def %s):  ",def_b);
gets(buff);
```

```
if(buff[0]!='\x0'){
con1=atof(buff);
strcpy(def_b,buff);
}
else {
con1=atof(def_b);
}
inp_con2:
buff[0]='\x0';
printf("Enter c-value(def %s):  ",def_c);
gets(buff);

if(buff[0]!='\x0'){
con2=atof(buff);
strcpy(def_c,buff);
}
else {
con2=atof(def_c);
}
}

**************************************************************************
The function eps() calculates for N = Cu or N = O the stopping cross section at
energy  = energy and returns the value to main()
**************************************************************************

double eps(N,energy)
int N;
double energy;
{
double epsilon=0.0;
int j;
energy=energy/1000.0;   /* convert E(keV) to E(MeV) */
for(j=0;j<6;++j)
epsilon+=a[N][j]*pow(energy,j);
epsilon*=1e-15;         /* epsilon (eV*cm^2/atom) */
return(epsilon);
}

**************************************************************************
The function brkt_eps() calculates for N = Cu or N = O the stopping cross
section at energy  = energy and returns the value to main()
**************************************************************************

double brkt_eps(k,angle,ep_i,ep_o)
double k,angle,ep_i,ep_o;
{
double bk_eps=0.0;
bk_eps=(k*ep_i+(ep_o/cos(pi-angle)));
return(bk_eps);
}
```

```
***********************************************************************
The function inp_emprcl() queries the user for the value = val_str defnum
assessed from the n/m ratio the with option of choosing the default and resets the
default values each time a new value is entered.
***********************************************************************

double inp_emprcl(val_str,defnum)
char val_str[25];
int defnum;
{

***********************************************************************
The variable val is the user–input value which is passed back to main() and
emp_str[25] from which the converted val is taken.
***********************************************************************

double val;
char emp_str[25];
extern char def_emp[][];

inp_val:
printf("For oxide, enter %s (def %s): ",val_str,def_emp[defnum]);
emp_str[0]='\x0';
gets(emp_str);

if(emp_str[0]!='\x0'){
val=atof(emp_str);
strcpy(def_emp[defnum],emp_str);
}
else
val=atof(def_emp[defnum]);
return(val);
}

***********************************************************************
The function write_file() prompts the user to type a file name for the output files
of the SEA or SMEA ratio–versus–thickness data. The default is reset and this
file name is returned to main upon valid entry.
***********************************************************************

void write_file(tp_str,which)
char tp_str[30];
char which[10];
{
extern char outfile[],def_app[];
control:
outfile[0]='\x0';
printf("Enter %s spectrum text file name\n",tp_str);
printf("in the form : %s",which);
gets(outfile);
```

```
if(outfile[0]=='\x0')
strcpy(outfile,def_app);
else
strcpy(def_app,outfile);
}
```

End of Document